Koupaei-Abyazani, Nikaan; Burdun, Iuliia; Desai, Ankur R.; Hergoualc'h, Kristell; Hirano, Takashi; Melling, Lulie; Swails, Erin; Ing Tang, Angela Che; Wong, Guan Xhuan

Tropical Peatland Water Table Estimations From Space

Published in:
Journal of Geophysical Research: Biogeosciences

DOI:
10.1029/2024JG008116

Published: 01/06/2024

Document Version
Publisher's PDF, also known as Version of record

JGR Biogeosciences

RESEARCH ARTICLE
10.1029/2024JG008116

Tropical Peatland Water Table Estimations From Space

Nikaan Koupaei-Abyazani[1], Iuliia Burdun[2], Ankur R. Desai[1], Kristell Hergoualc'h[3,4], Takashi Hirano[5], Lulie Melling[6], Erin Swails[7], Angela Che Ing Tang[8], and Guan Xhuan Wong[6]

[1]Department of Atmospheric and Oceanic Sciences, University of Wisconsin-Madison, Madison, WI, USA, [2]School of Engineering, Aalto University, Espoo, Finland, [3]Center for International Forestry Research (CIFOR), Lima, Peru, [4]Centre de coopération International en Recherche Agronomique pour le Développement (CIRAD) UMR Eco&Sols, Montpellier, France, [5]Research Faculty of Agriculture, Hokkaido University, Sapporo, Japan, [6]Sarawak Tropical Peat Research Institute, Kota Samarahan, Malaysia, [7]Center for International Forestry Research (CIFOR), Bogor, Indonesia, [8]Department of Environmental Sciences, University of Toledo, Toledo, OH, USA

Abstract Tropical peatlands store copious amounts of carbon (C) and play a critical role in the global C cycle. However, this C store is vulnerable to natural and anthropogenic disturbances, leading these ecosystems to become weaker C sinks or even net C sources. Variabilities in water table (WT) greatly influence the magnitude of greenhouse gas flux in these biomes. Despite its importance in C cycling, observations of the spatiotemporal dynamics of tropical peatland WT are limited in spatial extent and length. Here, we use in situ WT measurements from tropical peatlands in Indonesia, Malaysia, and Peru to evaluate the satellite-based Optical Trapezoid Model (OPTRAM). The model uses the pixel distribution in the shortwave infrared transformed reflectance and normalized difference vegetation index (NDVI) space to calculate indices that are then compared against in situ WT data. 30-m resolution Landsat 7 and Landsat 8 images were utilized for model parameterization. We found OPTRAM to best capture tropical peatland WT dynamics in minimally forested and non-forested areas (low to intermediate NDVI) ($0.7 < R < 1$) using the "best pixel" approach (the pixel with the highest Pearson-R correlation value). In areas with relatively higher NDVI, OPTRAM index did not correlate with WT (average R of -0.04 to 0.24), likely due to trees being less sensitive to WT fluctuations. OPTRAM shows potential for reliably estimating tropical peatland WT without the need for direct measurements, which is challenging due to site remoteness and harsh conditions.

Plain Language Summary Tropical peatlands store copious amounts of carbon in their soil and biomass. The position of the water table (WT) relative to the soil surface plays a large role in how much greenhouse gases (GHGs) (i.e., carbon dioxide, methane, and nitrous oxide) is emitted or taken up and may also give insight into areas most vulnerable to fire. Therefore, estimating tropical peatland WT fluctuations over space and time is essential for understanding the global carbon and GHG budgets. Due to harsh environmental conditions and site remoteness, direct measurements of tropical peatland WT are limited in spatial extent and length. As a result, other methods must be developed to estimate the spatiotemporal variability of this parameter. Through manipulation of satellite surface reflectance, we demonstrate the feasibility of estimating fluctuations in tropical peatland WT from space. This method is tested on sites spanning Peru, Indonesia, and Malaysia. We find that WT fluctuations are accurately quantified over areas that are minimally forested or non-forested. Our findings provide a pathway to map tropical peatland WT from space leading to improved understanding of WT-dependent processes such as GHG emissions and fire risk, both of which contribute greatly to global climate change.

Key Points:

- OPTRAM is capable of accurately capturing the temporal variability of tropical peatland water table
- OPTRAM performs optimally over minimally forested and non-forested areas

Supporting Information:

Supporting Information may be found in the online version of this article.

Correspondence to:

N. Koupaei-Abyazani,
nikaan.koupaei@gmail.com

Citation:

Koupaei-Abyazani, N., Burdun, I., Desai, A. R., Hergoualc'h, K., Hirano, T., Melling, L., et al. (2024). Tropical peatland water table estimations from space. *Journal of Geophysical Research: Biogeosciences*, *129*, e2024JG008116. https://doi.org/10.1029/2024JG008116

Received 7 MAR 2024
Accepted 28 MAY 2024

Author Contributions:

Conceptualization: Nikaan Koupaei-Abyazani, Iuliia Burdun
Data curation: Kristell Hergoualc'h, Takashi Hirano, Lulie Melling, Guan Xhuan Wong
Formal analysis: Nikaan Koupaei-Abyazani
Funding acquisition: Kristell Hergoualc'h, Takashi Hirano, Lulie Melling, Guan Xhuan Wong
Investigation: Nikaan Koupaei-Abyazani
Methodology: Nikaan Koupaei-Abyazani, Iuliia Burdun
Project administration: Nikaan Koupaei-Abyazani
Software: Nikaan Koupaei-Abyazani
Supervision: Ankur R. Desai
Validation: Nikaan Koupaei-Abyazani
Visualization: Nikaan Koupaei-Abyazani
Writing – original draft: Nikaan Koupaei-Abyazani
Writing – review & editing: Nikaan Koupaei-Abyazani, Iuliia Burdun,

1. Introduction

Tropical peatlands contain ~20% of the global peatland carbon (C) stock (Leifeld & Menichetti, 2018; Page et al., 2011) despite covering ~12% of the global peatland area (Dohong et al., 2017; Joosten, 2009; Melton et al., 2022; Xu et al., 2018). These biomes act as large reservoirs for C and play a critical role in the global C cycle (Page et al., 2011; Ribeiro et al., 2021). Changes in peatland WT are documented to govern GHG flux variability, especially in tropical regions where there is ample precipitation (Adeolu et al., 2015; Hergoualc'h et al., 2023; Hirano et al., 2014, 2015; Holden et al., 2004; Kwon et al., 2013; Rosenberry et al., 2006; Strack et al., 2005; Taufik et al., 2022, 2023). Carbon dioxide (CO_2) fluxes are recorded to be greater when WT is lowered, while methane (CH_4) fluxes increase at persistently high WT (Hoyos-Santillan et al., 2019; Wong

Ankur R. Desai, Kristell Hergoualc'h, Takashi Hirano, Lulie Melling, Erin Swails, Angela Che Ing Tang, Guan Xhuan Wong

et al., 2020). Nitrous oxide (N_2O) is emitted in both drained and undrained peatlands as it is produced through nitrification in aerobic conditions and denitrification in anaerobic conditions (Parn et al., 2018; Swails et al., 2021). The high dependency of GHG fluxes on WT suggests that rewetting drained tropical peatlands may aid in reducing CO_2 emissions or enhancing sequestration (Lestari et al., 2022). The associated risk of increased CH_4 emissions is low and, therefore, unlikely to negate CO_2 emission reductions (Hergoualc'h & Verchot, 2012; Jauhiainen et al., 2008).

Most peatland soils are characterized by their high porosity, allowing for high water storage capacity and high hydraulic conductivity (Evers et al., 2017; Huat et al., 2011; Melling, 2016; Taufik et al., 2022). Drastic change in WT has been documented to have effects on peat bulk density (Hooijer et al., 2012), hydraulic conductivity (Price, 2003), subsidence (Wösten et al., 1997), and surface-layer oxidation (Hooijer et al., 2012). This is especially the case for tropical peatlands during El Niño events (Khakim et al., 2020).

In addition, low WT leads to decreases in soil moisture and puts the aerated layer of peat at risk of fire (Dadap et al., 2019; Wösten et al., 2008), especially during the dry season and associated El Niño events in Southeast Asia. This can lead to extended smoldering periods (Turetsky et al., 2015) and extreme C emissions (Christian, 2003; Kuwata et al., 2017; Parker et al., 2016; Stockwell et al., 2014) which poses a serious health risk due to transboundary haze episodes (Cheong et al., 2019; Davies, 1999; Gaveau et al., 2014; Promsiri et al., 2023; Varkkey, 2013). Furthermore, fires can have large effects on hydrologic stability through the burning of low-density surface-layer peat (Thompson & Waddington, 2013). There is evidence, though, that peatland restoration by rewetting an area may reduce fire hazard (Taufik et al., 2023).

Despite its environmental impact, the quantification of tropical peatland WT variability has not been well-documented relative to peatlands in temperate and boreal regions. To date, continuous ground-based WT observations are scarce, and those that do exist are spatially and temporally limited (Busman et al., 2023; Dargie et al., 2017; Hergoualc'h et al., 2020; Hirano et al., 2012; Swails et al., 2021; Tang et al., 2018; Wright et al., 2013). Therefore, the spatiotemporal variability of tropical peatland WT is largely unknown, increasing uncertainties in all WT-dependent variables. As a result, it is crucial to resolve WT dynamics at high spatial resolution across a broad area to better understand its regional and local effects on GHG emissions and fire.

Some studies have purely used synthetic aperture radar (SAR) to monitor peatland WT (Bechtold et al., 2018; Kim et al., 2017), while several more have focused on only using optical approaches (Harris & Bryant, 2009; Kalacska et al., 2018; Meingast et al., 2014; Šimanauskienė et al., 2019). One study has used machine learning to predict spatiotemporal variability in tropical peatland WT (Hikouei et al., 2023), while another monitored this parameter via variabilities in Earth's gravitational field (Swails et al., 2019).

Tropical peatland hydrology has been simulated in a scalar-based hydrologic model (Cobb & Harvey, 2019), process-based land models (Apers et al., 2022; Mezbahuddin et al., 2015) and also utilized for reproducing effects on GHG fluxes (Mezbahuddin et al., 2014). While these efforts have proven somewhat successful, restrictions persist due to limited spatial estimations of tropical peatland hydrological parameters. The Optical Trapezoid Model (OPTRAM) (Sadeghi et al., 2017) may aid in closing this gap by providing reliable estimates of WT in these systems, and therefore reducing model uncertainty and improving our understanding of peatland hydrology in the tropics.

Here, we test the effectiveness of OPTRAM (Sadeghi et al., 2017) in capturing temporal, spatial, and spatiotemporal WT variability for the first time in tropical peatlands. OPTRAM, originally developed for estimating soil moisture, has previously been shown to reliably retrieve water tables in boreal and temperate peatlands (Burdun, Bechtold, Sagris, Komisarenko, et al., 2020; Burdun, Bechtold, Sagris, Lohila, et al., 2020; Burdun et al., 2023; Räsänen et al., 2022). However, it is assumed that WT retrieval in forested tropical peatlands is weaker due to more dense vegetation cover, though this has not been evaluated. We use satellite images from the Landsat 8 Operational Land Imager Collection 2 Level 2 and Landsat 7 Enhanced Thematic Mapper Plus Collection 2 Level 2 Surface Reflectance Products as inputs and validate the model using in situ WT measurements from six tropical peatland sites in Southeast Asia (Sarawak, Malaysia and Central Kalimantan, Indonesia) and South America (Loreto, Peru) with various disturbance (i.e., drained, undrained, degraded, and converted). We set out to answer the following questions:

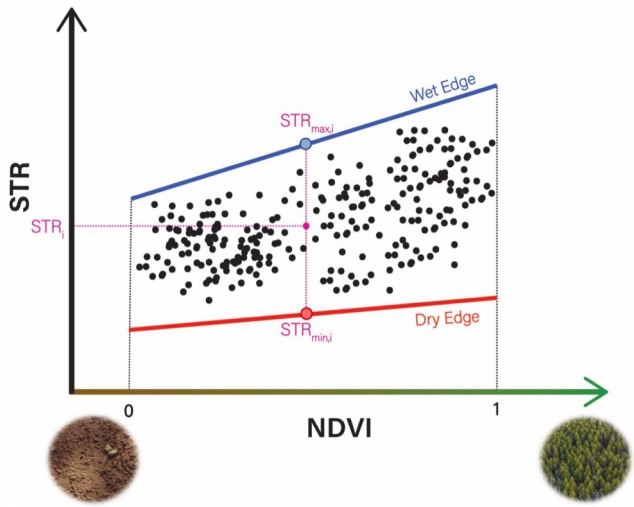

Figure 1. A diagram of the OPTRAM model. Individual pixels i (black dots) are plotted in the normalized difference vegetation index (NDVI) and shortwave infrared transformed reflectance (*STR*) space. Wet (blue line) and dry (red line) edges are determined through visual inspection. These edges are utilized in evaluating $STR_{max,i}$ and $STR_{min,i}$ for each pixel. STR_i represents the *STR* value for a given pixel. All three of these parameters are used in determining the OPTRAM index for each pixel via Equation 5.

- Is OPTRAM capable of capturing temporal variations in tropical peatland WT?
- Does OPTRAM performance depend on the area where applied and/or extent of disturbance?
- Does OPTRAM performance depend on surface vegetation density?

2. Methods

2.1. The Optical Trapezoid Model (OPTRAM)

OPTRAM was first proposed by Sadeghi et al. (2017) in response to the Thermal-Optical Trapezoid Model's shortcomings (Figure 1).

OPTRAM uses optical remote sensing data and relies on pixel distributions within the shortwave infrared transformed reflectance (STR) and normalized difference vegetation index (NDVI) space (Figure 2). NDVI acts as an indicator of vegetation density and health and is determined based on the interactions between light and chlorophyll (Zeng et al., 2022):

$$\text{NDVI} = \frac{S_{NIR} - S_{Red}}{S_{NIR} + S_{Red}} \tag{1}$$

where S_{NIR} and S_{Red} represent the near-infrared and red surface reflectance, respectively. STR is a manipulation of the shortwave infrared (SWIR) surface reflectance:

$$\text{STR} = \frac{(1 - S_{SWIR})^2}{2S_{SWIR}} \tag{2}$$

where S_{SWIR} is the SWIR surface reflectance.

The STR-NDVI pixel distribution is used to define the dry and wet edges of the space (Figure 1), with each edge characterized by a linear equation:

$$STR_{min,i} = m_{min}\text{NDVI} + b_{min} \tag{3}$$

$$STR_{max,i} = m_{max}\text{NDVI} + b_{max} \tag{4}$$

$STR_{min,i}$, m_{min}, and b_{min} are the STR value, slope, and intercept for the dry edge, respectively. The same holds for $STR_{max,i}$, m_{max}, and b_{max} but for the wet edge. *i* indicates an arbitrary pixel in the STR-NDVI space within the dry and wet edges. These edges are typically drawn through visual inspection (Chen et al., 2020; Sadeghi et al., 2017) and create a trapezoid around the pixel distribution (Figure 2).

After parameterization, $STR_{min,i}$ and $STR_{max,i}$ are used to calculate the OPTRAM index via the following equation:

$$\text{OPTRAM Index} = \frac{STR_i - STR_{min,i}}{STR_{max,i} - STR_{min,i}} \tag{5}$$

2.2. Satellite Images

For sites with in situ WT data during and after 2014 (Table 1), input variables for Equations 1 and 2 were provided by the Landsat 8 Operational Land Imager Collection 2 Level 2 Surface Reflectance Product (L8 OLI). L8 OLI provides ground-level spectral reflectance across nine spectral bands at 30-m resolution every 16 days (Vermote et al., 2016). L8 OLI images were downloaded from the USGS Earth Explorer server (https://earthexplorer.usgs.gov) and the red, near-infrared (NIR), and SWIR surface reflectances were utilized for OPTRAM parameterization. This corresponds to bands 4 (0.64–0.67 μm), 5 (0.85–0.88 μm), and 7 (2.11–2.29 μm) in L8 OLI,

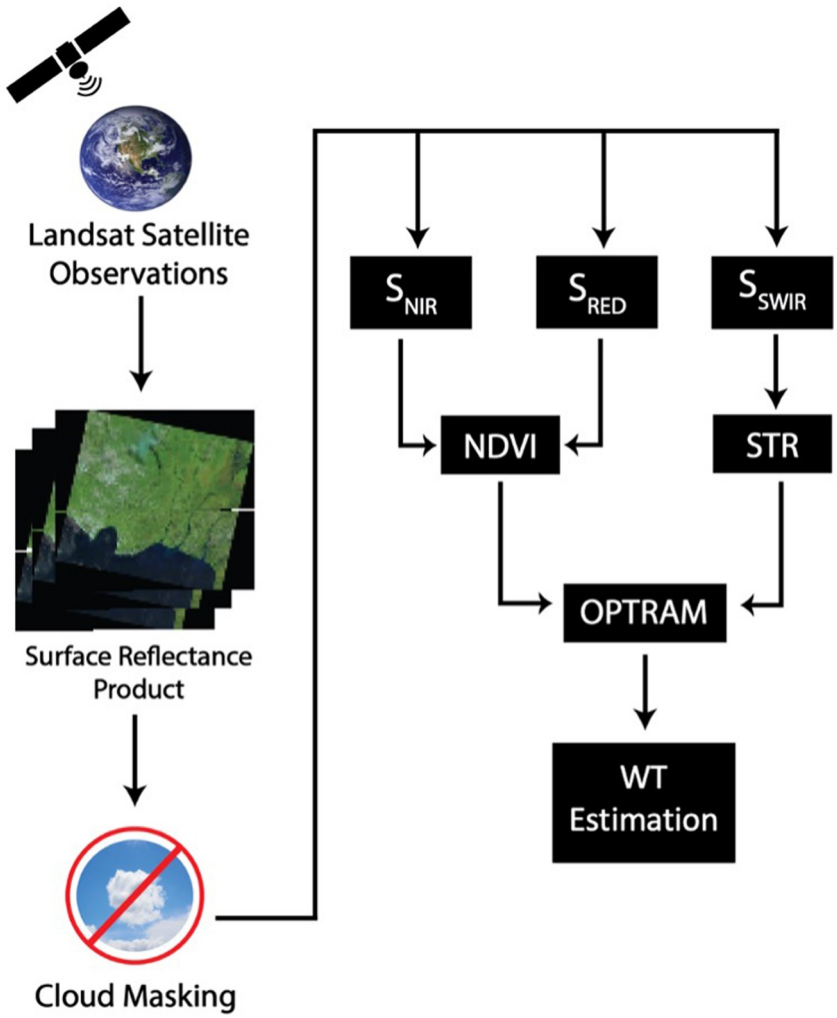

Figure 2. Flowchart illustrating steps followed for calculating OPTRAM and obtaining a WT estimation.

respectively. Additionally, bands 4 and 5 were used to calculate NDVI, while band 7 was used to compute STR (Figure 2).

For sites with in situ data before 2014 (when L8 OLI was not yet online) (Table 1), we used the Landsat 7 Enhanced Thematic Mapper Plus Collection 2 Level 2 Surface Reflectance Product (L7 ETM+) (Masek et al., 2006). Like L8 OLI, L7 ETM+ provides ground-level spectral reflectance at 30-m resolution with a 16-day repeat cycle but has only eight spectral bands compared to L8 OLI's nine. These images were also downloaded from the USGS Earth Explorer server and were manipulated such that L7 ETM+ images overlapped with L8 OLI images to ensure similar regional coverage. The bands used from L7 ETM+ were bands 3 (red; 0.63–0.69 μm), 4 (NIR; 0.77–0.90 μm), and 7 (SWIR; 2.08–2.35 μm). L7 ETM+ and L8 OLI bands were not cross-harmonized. It is important to note that the Scan Line Corrector, which compensates for the forward motion of the Landsat 7 satellite, failed permanently in May 2003. As a result, the image area was duplicated. These duplicated areas have been removed, causing data gaps. Despite removing duplicated areas, about 78% of the pixels are still available (https://www.usgs.gov/landsat-missions/landsat-7). All calculations and analyses were conducted in Python (version 3.8.13 and 3.9.18).

Many L7 ETM+ and L8 OLI images contain cloudy pixels, especially in the tropics. This blocks specific wavelengths from reaching the instrument, and these pixels are therefore deemed unusable for OPTRAM. To account for this, we only used images with a cloud cover of 50% or less as determined by the "C function of mask" algorithm (Foga et al., 2017). To further omit cloudy L8 OLI pixels, we filtered pixels via the product's quality

Table 1
Site Information Including Coordinates, Years of Data Used for Validation, Publication Source, Nature of Disturbance, and Dominant Vegetation Cover

Country	Site ID	Coordinates	Years used	Publication	Nature of disturbance	Dominant vegetation cover
Indonesia	IN-undrained	2.32°S, 113.90°E	2015–2018	Hirano et al. (2012)	Selectively logged until late 1990s; Designated a National Park in 2006; Little drainage due to network of small canals	*Combretocarpus rotundatus* *Cratoxylum arborescens* *Buchanania sessifolia* *Tetramerista glabra*
	IN-drained	2.35°S, 114.04°E	2013–2017	Hirano et al. (2012)	Selectively logged until late 1990s; Drained	*Combretocarpus rotundatus* *Cratoxylum arborescens* *Buchanania sessifolia* *Tetramerista glabra*
Peru	PE-mDeg	3.8394°S, 73.3250°W	2015–2018	Hergoualc'h et al. (2020)	Moderately degraded (timber harvesting and palm cutting for fruit harvesting)	*Mauritia flexuosa*
	PE-hDeg	3.80898°S, 73.30713°W	2014–2018	Hergoualc'h et al. (2020)	Heavily degraded (timber harvesting and palm cutting for fruit harvesting)	*Mauritia flexuosa* *Cecropia membranacea*
Malaysia	MA-undrained	1.4536°N, 111.1494°E	2011–2014	Tang et al. (2020)	Logged before 2000; A totally protected area since 2000	*Shorea albida* *Lithocarpus* *Litsea* *Stemonurus*
	MA-converted	2.1860°N, 111.8459°E	2018–2019	Nishina et al. (2023)	Oil Palm Plantation converted from peat swamp forest in 2001	*Elaeis guineensis*

assurance flags outlined in the Landsat 8–9 Collection 2 Level 2 Science Product Guide version 5 (Masek et al., 2006). Only pixels labeled as "clear" were kept in our analysis. To further constrain the amount of cloudy L7 ETM+ pixels, we only kept pixels characterized as "low cloud confidence" according to the Landsat 4–7 Collection 2 Level 2 Science Product Guide version 4 (Cook, 2014; Cook et al., 2014; Vermote et al., 2016). These measures allowed OPTRAM to be run with largely unobstructed surface reflectance values, resulting in more reliable OPTRAM indices and, consequently, a better representation of surface water content.

2.3. Site Descriptions

OPTRAM was validated using in situ WT from sites in Indonesia (Hirano et al., 2012, 2015), Malaysia (Nishina et al., 2023; Tang et al., 2020), and Peru (Hergoualc'h et al., 2020). The Indonesian peat swamp forest sites are located near Palangkaraya in Central Kalimantan, Indonesia and vary in disturbance. One is relatively intact with little drainage (IN-undrained; 2.32°S, 113.90°E), while the other is drained (IN-drained; 2.35°S, 114.04°E) (Ohkubo et al., 2021) (Figures 3 and 4). Both were selectively logged until the late 1990s. IN-undrained resides in an area designated a National Park in 2006. The undrained site contains a network of small canals while the drained site contains a large canal (25 m wide and 3.5–4.5 m deep) which is ∼400 m from the site (Hirano et al., 2012). At these two sites, WT was measured half-hourly via a water level logger (DL/N; Sensor Technik Sirnach AG, Sirnach, Switzerland or DCX-22 VG; Keller AG, Winterthur, Switzerland) (Hirano et al., 2007; Ohkubo et al., 2021).

Two other sites are located in Malaysia. One is an undrained peat swamp forest (PSF) in Maludam National Park in the Betong Division of Sarawak, Malaysia (MA-undrained; 1.4536°N, 111.1494°E) (Tang et al., 2020). This site has been subject to large-scale protection measures since 2000, and presents a WT near or above the peat surface (Tang et al., 2020). WT was measured on a half-hourly basis via a water level logger (DL/N 70 STS Sensor, Technik Sirnach AG) (Tang et al., 2020). The other site is an oil palm plantation converted from peat swamp forest in 2001 (MA-converted; 2.1860°N, 111.8459°E) (Nishina et al., 2023) (Figures 3 and 4). MA-converted contains numerous drainage ditches which were likely used to facilitate oil palm plantation establishment (Nishina et al., 2023). The water table at MA-converted was measured every half hour by a piezometer (HOBO, Onset, Bourne, MA, USA).

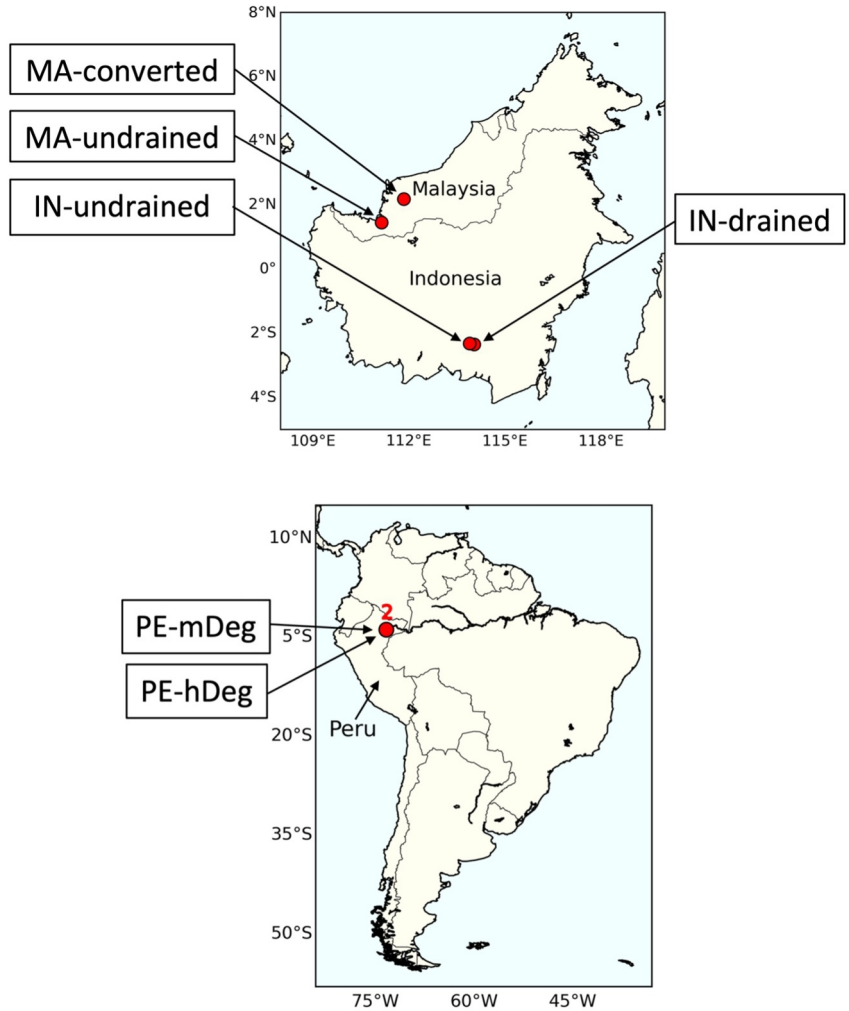

Figure 3. Locations of sites used for OPTRAM validation.

The Peruvian sites are located in the Northern Peruvian Amazon in Loreto province and comprise a moderately degraded (PE-mDeg; 3.8394°S, 73.32502°W) and heavily degraded (PE-hDeg; 3.80898°S, 73.30713°W) PSF (Hergoualc'h et al., 2020) (Figures 3 and 4). Both sites were subject to *M. flexuosa* palm cutting for fruit harvesting and logging. The WT relative to the soil surface was monitored in a perforated polyvinyl chloride tube (diameter: 5 cm; length: 1.5 m) installed permanently in the soil (Hergoualc'h et al., 2020). WT data at PE-mDeg and PE-hDeg were computed to site-scale using the relative proportion of area occupied by cut palms on a hummock and adjacent hollow, and live palms on a hummock and adjacent hollow (Hergoualc'h et al., 2020; Hergoualc'h, 2024).

The site years used for OPTRAM validation were 2015–2018 for IN-undrained, 2013–2017 for IN-drained, 2011–2014 for MA-undrained, 2018–2019 for MA-converted, 2015–2018 for PE-mDeg, and 2014–2018 for PE-hDeg (Table 1). Lack of continuous daily data for PE-mDeg and PE-hDeg forced us to use L8 OLI images that did not align exactly with dates of in situ WT data. Although WT did not substantially vary on small timescales (i.e., days to weeks) (Hergoualc'h et al., 2020), we caution that results at these sites may be affected by this misalignment to a certain degree.

2.4. Data Computation and Statistical Testing

To assess OPTRAM's capability for reproducing the variability in WT (and not exact values), we constructed a matrix of spatially identical in situ WT values covering a 5–9 km radius centered around the location of WT

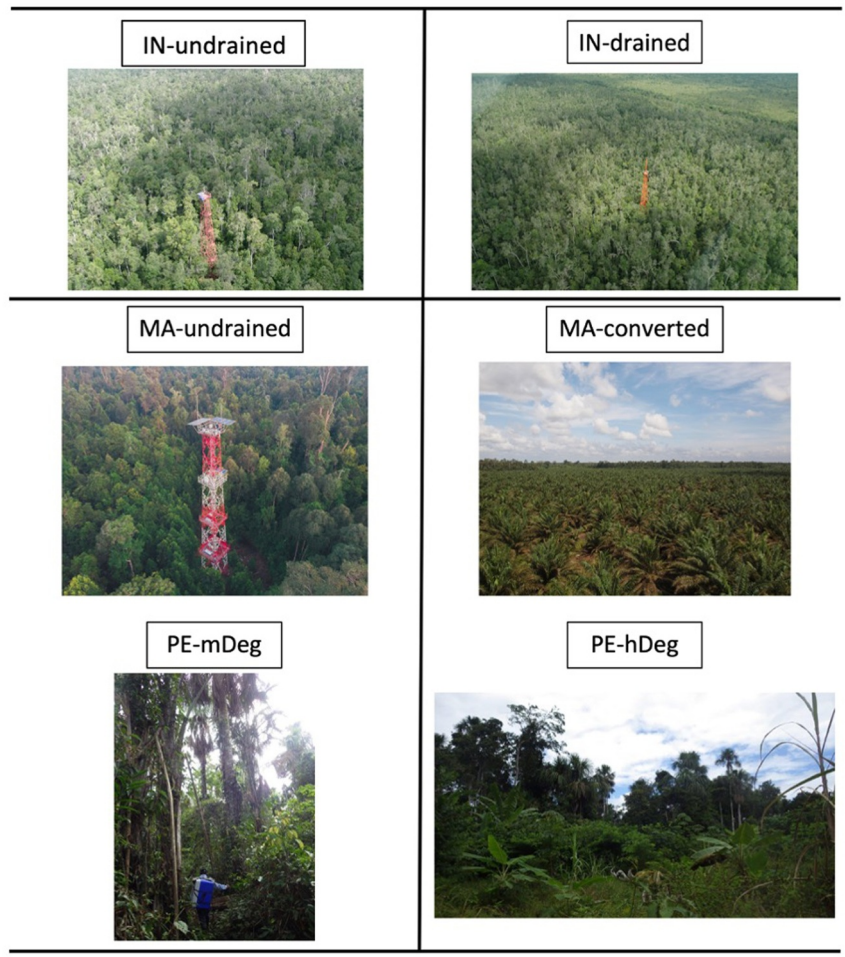

Figure 4. Pictures of sites used for OPTRAM validation.

measurement. We also created a matrix of OPTRAM indices with values varying based on topographical characteristics (see summarized workflow in Figure 2). The Pearson correlation coefficient (R) was utilized to assess OPTRAM's effectiveness in capturing temporal variability in WT:

$$R = \frac{\sum_{i=1}^{N}(y_i - \bar{y})(p_i - \bar{p})}{\sqrt{\sum_{i=1}^{N}(y_i - \bar{y})^2 \sum_{i=1}^{N}(p_i - \bar{p})^2}} \quad (6)$$

where y_i and p_i represent the in situ WT observation and OPTRAM estimation at time index i, respectively. $\bar{y}$ denotes the mean of the observations while $\bar{p}$ indicates the mean of the estimatis. N is the number of data points. The per-pixel correlation was then projected onto the map of the site to create a correlation map. Model performance was evaluated using the "best pixel" approach (Burdun, Bechtold, Sagris, Lohila, et al., 2020) which involves choosing the highest R-value to represent the correlation between OPTRAM index and in situ WT.

Due to cloud masking, the Pearson-R correlation value for each pixel was not calculated with the same number of data points. To test the impact of this issue on results, we constructed a spatial distribution of "number of data points" for each pixel and compared it with each site's Pearson-R correlation map. In addition, the scarcity of long-term data records further limited the number of data points that could be included. Therefore, we set a threshold for the number of data points to be included in certain sites when identifying the "best pixel." This was done to omit erroneously high Pearson-R values due to a low number of data points. For MA-converted, PE-

mDeg, and PE-hDeg, the "best pixel" was determined from a pool of pixels with a number of data points ≥13. For IN-drained and MA-undrained, the threshold was set at 21 and 17, respectively. There was no threshold for other sites due to the relatively high number of data points at the "best pixel" location.

2.5. OPTRAM and Vegetation Density

In a previous study in northern peatlands (Burdun, Bechtold, Sagris, Lohila, et al., 2020), the performance of OPTRAM was optimal in areas with minimal shrubs or trees. To test this in tropical peatlands, we used NDVI as an indicator for vegetation density (Zaitunah et al., 2018). NDVI's assessment of vegetation "greenness" is correlated with vegetation crown density, allowing its use as a proxy for vegetation density (Zaitunah et al., 2018). Afterward, we assessed its relationship with the OPTRAM index-WT Pearson-R value on a per-pixel basis. High and low NDVI values represented high and low vegetation density, respectively. Since tropical PSF are characterized by evergreen vegetation, we calculated NDVI using only September surface reflectance values for each site. This month was chosen due to being at the end of the dry season and consequently creating conditions where satellite images are less likely to be obscured by cloud cover.

2.6. Testing Relationship Differences Between El Niño and Non-El Niño Years

The years of data used for four of the sites fell within the 2015–2016 strong El Niño year (IN-undrained, IN-drained, PE-mDeg, and PE-hDeg). However, only the IN-undrained and IN-drained sites were used since PE-mDeg and PE-hDeg did not have sufficient data for analysis. The El Niño period was defined to occur from January 2015 through March 2016. A two-sided *t*-test was used to calculate the 95% confidence interval for the slopes of El Niño and non-El Niño regression lines. Slopes were considered significantly different if 95% confidence intervals did not overlap with one another. These were applied to pixels with the first, second, and third largest Pearson-R value.

2.7. Uncertainty Analysis

We utilized a cross-validation approach to incorporate uncertainty in OPTRAM's ability for detecting changes in WT. The best pixel for each site was chosen for this analysis. We fitted a regression line using the "linregress" function from the "stats" module within the "SciPy" library in Python. The regression line was fitted using all but one single data point. We then calculated the difference between the observed and predicted OPTRAM index values. This was repeated for all data points. The mean absolute error (MAE) was then calculated as:

$$\mathrm{MAE} = \frac{\sum_{i=1}^{n} |x_i - y_i|}{n} \tag{7}$$

where x_i, y_i, and n represent the observed OPTRAM index value, predicted OPTRAM index value, and number of data points, respectively.

3. Results

3.1. OPTRAM Parameterization

We observed a positive relationship between the STR and NDVI across most sites, with varied type of relationship (i.e., linear, exponential, etc.) depending on the date (Figure 5). For example, Figure 5 shows a linear relationship between STR and NDVI at IN-undrained at the end of January and September 2018, while an exponential relationship was observed at the beginning of May and December 2018.

The STR value peaked within the dense pixel area at an NDVI of ~0.85–0.9 on all four different dates (Figure 5). The wet and dry edges were determined via visual inspection by drawing two lines such that, between them, a majority of the pixels were contained (Figure 5). This resulted in the following parameterization:

$$STR_{min,i} = (2.121)(\mathrm{NDVI}) - 0.296 \tag{8}$$

$$STR_{max,i} = (30.134)(\mathrm{NDVI}) + 5.856 \tag{9}$$

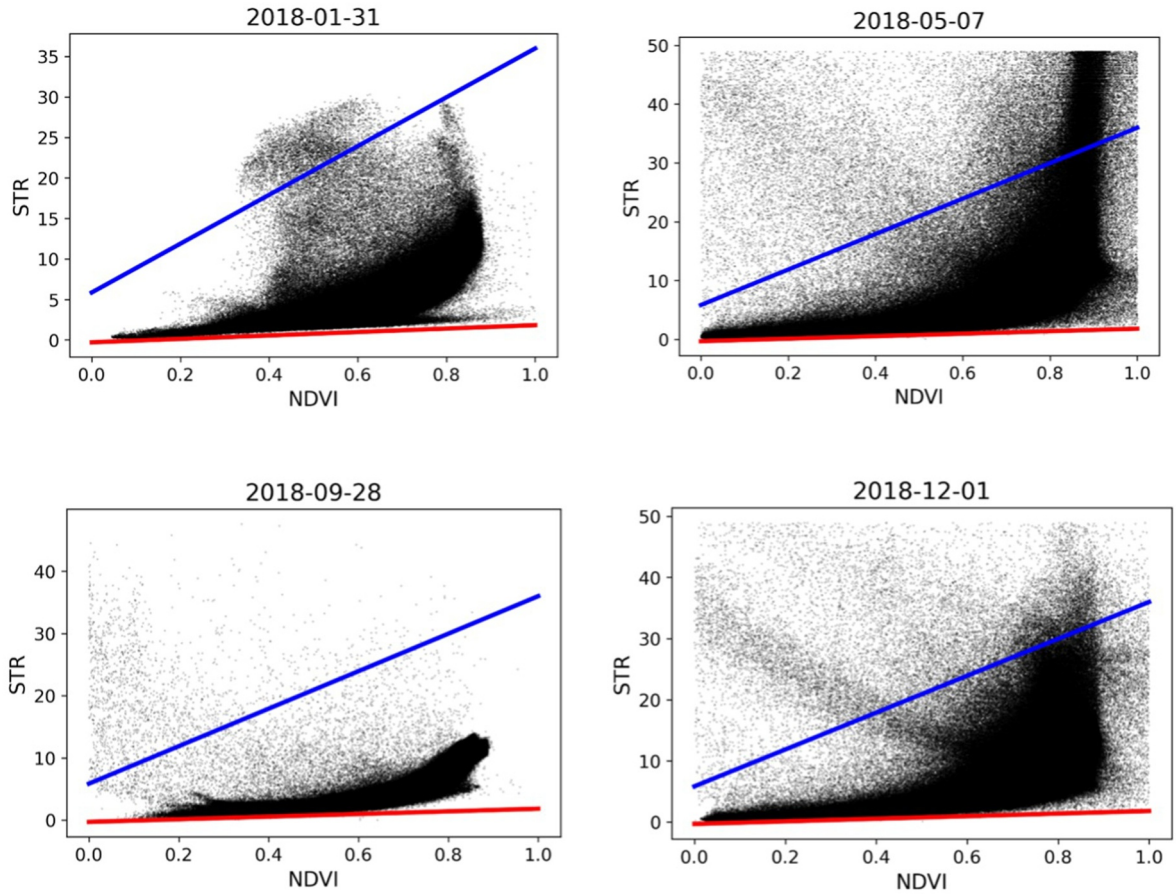

Figure 5. 30-m resolution Landsat 8 pixels plotted in the shortwave infrared transformed reflectance (STR) and normalized difference vegetation index (NDVI) space. Only four dates in 2018 are shown at IN-undrained to illustrate the diversity in pixel distributions. The wet edge is represented by the blue line and the dry edge is the red line. These were drawn through visual inspection such that most of the pixels resided between the two lines. Note that the slope and intercept of these lines remain constant for each date. m_{min}, b_{min}, m_{max}, and b_{max} were 2.121, −0.296, 30.134, and 5.856, respectively.

These values for m_{min}, b_{min}, m_{max}, b_{max} were used for all sites and dates. While images with cloud cover of 50% or less were retained for analysis, we did not further filter pixels using quality assurance flags at this stage.

3.2. In Situ WT Variability

In situ WT varied considerably over time at all sites. At IN-undrained, WT exhibited a distinct seasonal cycle, fluctuating between an average depth of ∼−60 cm and the peat surface, with the exception of the 2015 dry season (very strong El Niño year) when WT reached a depth as low as ∼140 cm below the peat surface (Hirano, 2023) (Figure 6). At IN-drained, similar temporal variability in WT was observed (Figure 6). At MA-undrained, WT had a seasonal cycle, with WT being mostly below the peat surface during the dry seasons and above during the wet seasons. From 2011 through 2014, WT varied between ∼−39 and ∼24 cm (Figure 6) (Melling & Wong, 2024).

The sampling frequency was lower at Peruvian sites, occurring monthly (we show every 2–5 months in Figure 6), compared to the daily sampling at IN-undrained and IN-drained (Hirano, 2023). At PE-mDeg, WT remained at or near the peat surface during the sampling period from 2015 to 2016 and increased to ∼20 cm in mid-2017 (Figure 6) (Hergoualc'h, 2024). Similarly, WT was close to the peat surface throughout 2015 and 2016 at PE-hDeg. However, in mid-2017, WT at PE-hDeg increased to ∼50 cm, concurrent with the increase observed at PE-mDeg (Figure 6) (Hergoualc'h, 2020; Hergoualc'h, 2024).

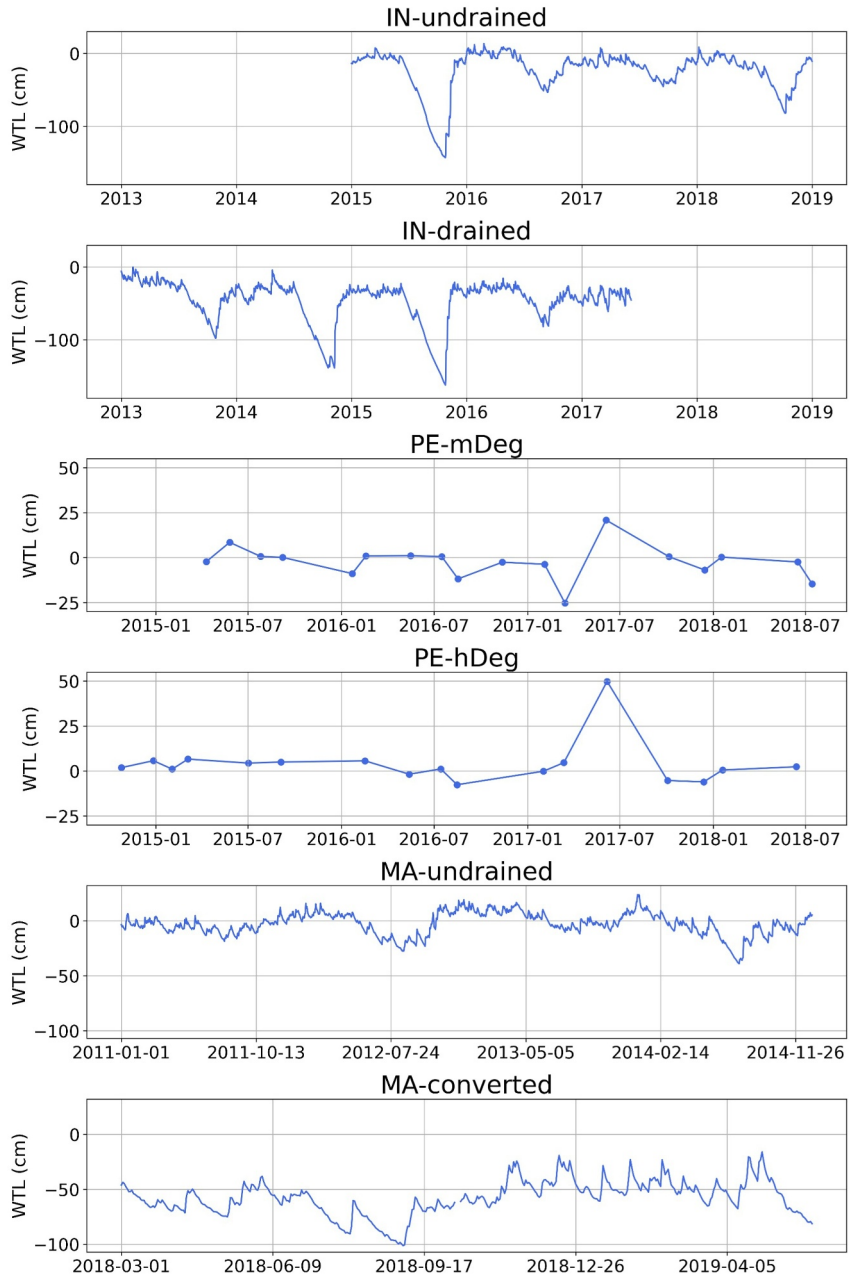

Figure 6. Time series of daily averaged in situ water table (WT) at the Indonesian and Malaysian sites. For Peruvian sites, time series shows the WT approximately every 2–5 months. A positive WT indicates a water table above the peat surface. Note that dates for IN-undrained and IN-drained and dates for PE-mDeg and PE-hDeg align. WT data used from Hirano et al. (2012), Tang et al. (2020), and Hergoualc'h et al. (2020).

3.3. Estimating Tropical Peatland WT Variability via OPTRAM

Overall, the performance of OPTRAM in reproducing the temporal variability of tropical peatland WT varied spatially and was largely dependent on the density of vegetation. At IN-undrained, the relationship between OPTRAM index and in situ WT greatly varied ($\sim -0.7 < R < \sim 0.95$). In areas with little to no vegetation, OPTRAM performance was optimal, with Pearson-R values $>\sim 0.6$ (Figure 7). Moreover, Pearson-R correlations of up to 0.94 were found, with the "best pixel" ($R = 0.94$; $p < 0.001$) located in an area with minimal vegetation cover. Conversely, no significant correlation was found at the location of in situ WT measurement where there was abundant tree cover ($R = -0.17$; $p > 0.05$).

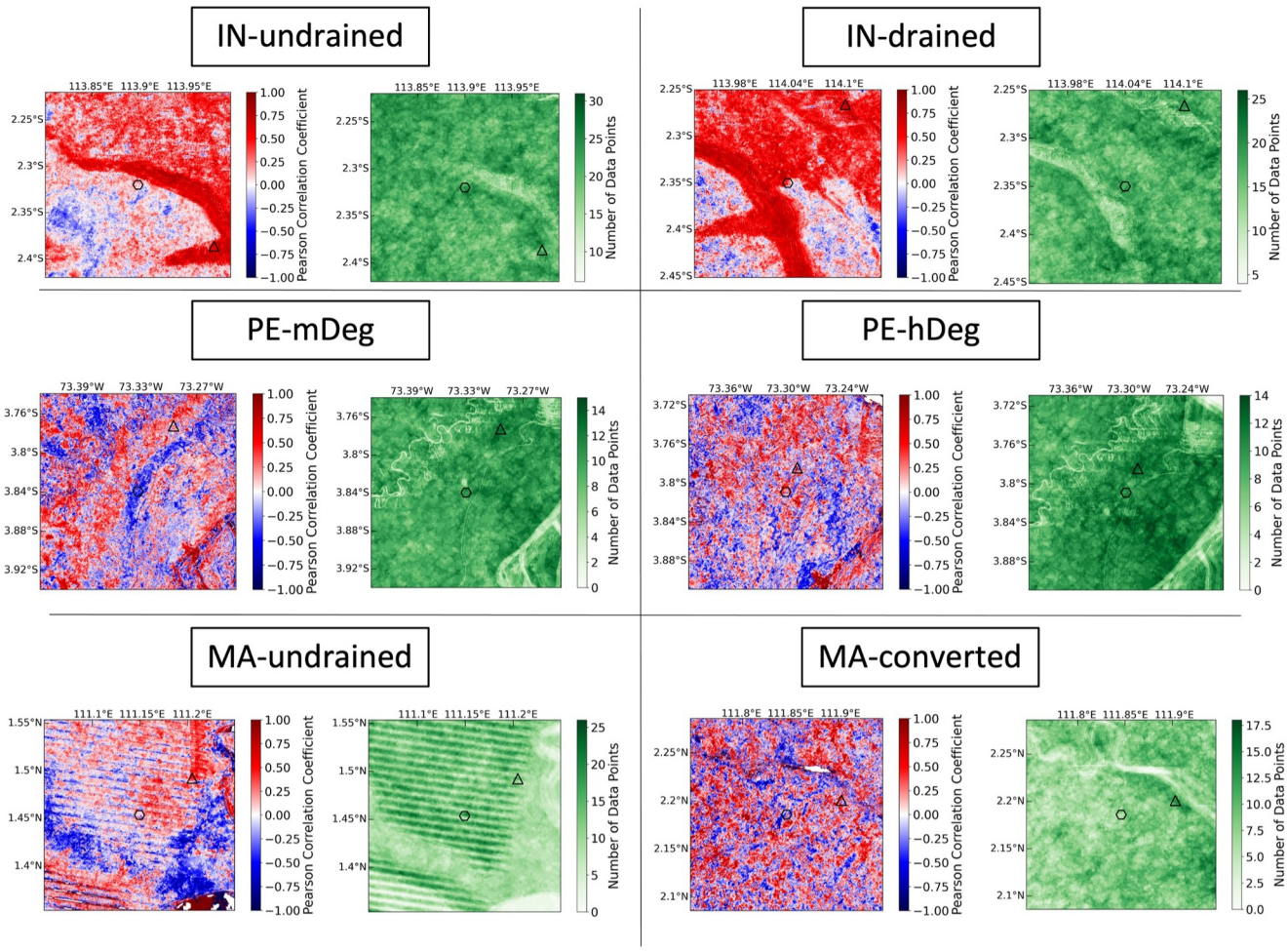

Figure 7. Pearson-R correlation values (30-m resolution) and number of data points (NDP) per pixel (30-m resolution) at all study sites. The middle hexagon is the location of in situ water table measurement and the triangle is the location of the "best pixel" (pixel with largest positive Pearson-R within the domain).

At IN-drained, a similar result was obtained. Areas with low vegetation cover were also areas where OPTRAM was best at detecting temporal WT variability (Figure 7). Areas with high vegetation showed spatially sporadic correlations ranging from $R = \sim -0.6$ to $R = \sim 0.5$ (Figure 7). At the location of in situ WT measurement, the R-value was 0.62 ($p < 0.05$; without outlier), with the "best pixel" yielding an R-value of 0.87 ($p < 0.001$; when only pixels with 21 or more data points were considered) (Figure 7).

For PE-mDeg, correlations were once again relatively high ($R > 0.5$) in areas with low vegetation cover (Figure 7). This was superimposed with areas that had zero correlation due to the presence of buildings and ponds. Areas with high vegetation cover were associated with sporadic correlations that ranged from $R = \sim -0.75$ to $R = \sim 0.5$) (Figure 7). OPTRAM did not capture WT variability at the location of WT measurement ($R = -0.32$; $p > 0.05$). The "best pixel" ($R = 0.82$; $p < 0.001$) was in an area with relatively minimal vegetation cover (Figure 7).

Correlation patterns at PE-hDeg varied drastically relative to that of PE-mDeg. Besides an area of high correlation values that was observed from the middle left section to the top middle section, there were no other notable patterns between vegetation density and correlation strength between OPTRAM index and in situ WT (Figure 7). A positive correlation was found at the location of WT measurement ($R = 0.57$; $p > 0.05$) (Figure 7). The "best pixel" ($R = 0.79$; $p < 0.05$; without outlier), in this case, should not be given credence due to the primarily disordered relationship between vegetation density and correlation strength.

Unlike other sites, MA-undrained showed higher correlations in the presence of moderate vegetation cover ($R = \sim 0.5$). The "best pixel" ($R = 0.49$; $p > 0.05$; without outlier) was in an area with relatively low vegetation cover. The location of WT measurement (Melling & Wong, 2024) was situated in an area with relatively high vegetation cover and yielded a correlation of $R = -0.17$; $p > 0.05$) (Figure 7).

Similar to PE-hDeg, the correlation distributions at MA-converted did not show a pattern between high and low vegetated areas (Figure 7). Therefore, the "best pixel" R-value ($R = 0.88$; $p < 0.001$) cannot be regarded as being an accurate representation of OPTRAM performance. At the location of WT measurement, the R-value was 0.007 with a corresponding p-value greater than 0.05 (Figure 7).

The "best pixel" scatterplots (Figure 8) show for all sites a fairly universal relationship between OPTRAM index and in situ WT, with an increase of OPTRAM index by ~0.1 for every ~20 cm increase in WT. This was true even for sites that had outliers.

3.4. NDVI's Influence on OPTRAM Performance

For IN-undrained and IN-drained, as NDVI increased, Pearson-R tended to decrease (Figure S1 in Supporting Information S1). The two Indonesian sites also experienced mostly positive Pearson-R values below an NDVI of ~0.6 (Figure S1 in Supporting Information S1). For PE-mDeg and PE-hDeg, the pixels did not show a noticeable trend, and instead showed Pearson-R values that ranged from ~−0.75 to 0.75 from an NDVI of ~0.15–0.85 (Figure S1 in Supporting Information S1). However, at an NDVI of ~0.85, most pixels were situated within a Pearson-R value of −0.5 to 0.5 (Figure S1 in Supporting Information S1). MA-undrained showed little relationship between Pearson-R and NDVI. Most pixels were located at NDVI greater than ~0.6 and there was a wide spread of Pearson-R values above an NDVI of ~0.7 (Pearson-R value range of ~−0.7 to 0.75) (Figure S1 in Supporting Information S1). MA-converted, like PE-mDeg and PE-hDeg, did not show a noticeable trend, with Pearson-R values ranging from ~−0.6 to ~−0.85 across most NDVI values (mostly when NDVI > ~0.6) (Figure S1 in Supporting Information S1).

At all sites, pixels with NDVI values 0–0.4 and 0.4–0.7 also had higher average correlation values relative to pixels with NDVI values between 0.7 and 1 (Figure 9). At IN-undrained, the average R values were approximately the same for NDVI values 0–0.4 and 0.4–0.7 (average $R = \sim 0.35$). However, for NDVI values between 0.7 and 1, the average R value dropped to ~0.14. IN-drained experienced a similar relationship, with an average R value of ~0.4 for NDVI of 0–0.4 and 0.4–0.7 and an average R value of ~0.24 for NDVI between 0.7 and 1. For PE-mDeg, the NDVI range 0.4–0.7, had the largest average R value (average $R = \sim 0.14$). This was followed by NDVI 0–0.4 (average $R = \sim 0.1$) and 0.7–1 (average $R = \sim 0.01$). While PE-hDeg showed positive average R values for NDVI thresholds 0–0.4 and 0.4–0.7 (average R values of ~0.01 and ~0.04, respectively), the NDVI threshold of 0.7–1 yielded a negative average R value of ~−0.035). Lastly, MA-undrained and MA-converted showed similar average R-values for each NDVI threshold. An average R value of ~0.12 for an NDVI range of 0–0.4 was found for both sites. For NDVI threshold 0.4–0.7, average R values of ~0.175 and ~0.16 were found at MA-undrained and MA-converted, respectively. For NDVI threshold 0.7–1, an average R value of ~0.075 was observed at MA-undrained, while an average R value of ~0.07 was found at MA-converted.

3.5. The Number of Data Points and OPTRAM Performance

The number of data points per pixel (NDP) generally did not impact the correlation strength between OPTRAM index and in situ WT. The distribution was mainly a result of filtering cloudy pixels via the "C Function of Mask" algorithm to ensure pixel quality. Moreover, L7 ETM+ images were subject to data gaps due to permanent failure of the Scan Line Corrector.

At IN-undrained, there was a mixture of low and high NDP where high correlations were observed ($R > \sim 0.6$) (Figure 7). This did not, however, influence the strength of correlation (Figure 7). This was also the case for IN-drained. The remaining sites had lower NDP throughout the landscape relative to IN-undrained and IN-drained (with the exception of MA-undrained) (Figure 7). Therefore, we applied thresholds to use for NDP to obtain reliable results for the "best pixel" location. With that said, distributions of NDP on a site-by-site basis also did not greatly affect correlation strength (Figure 7).

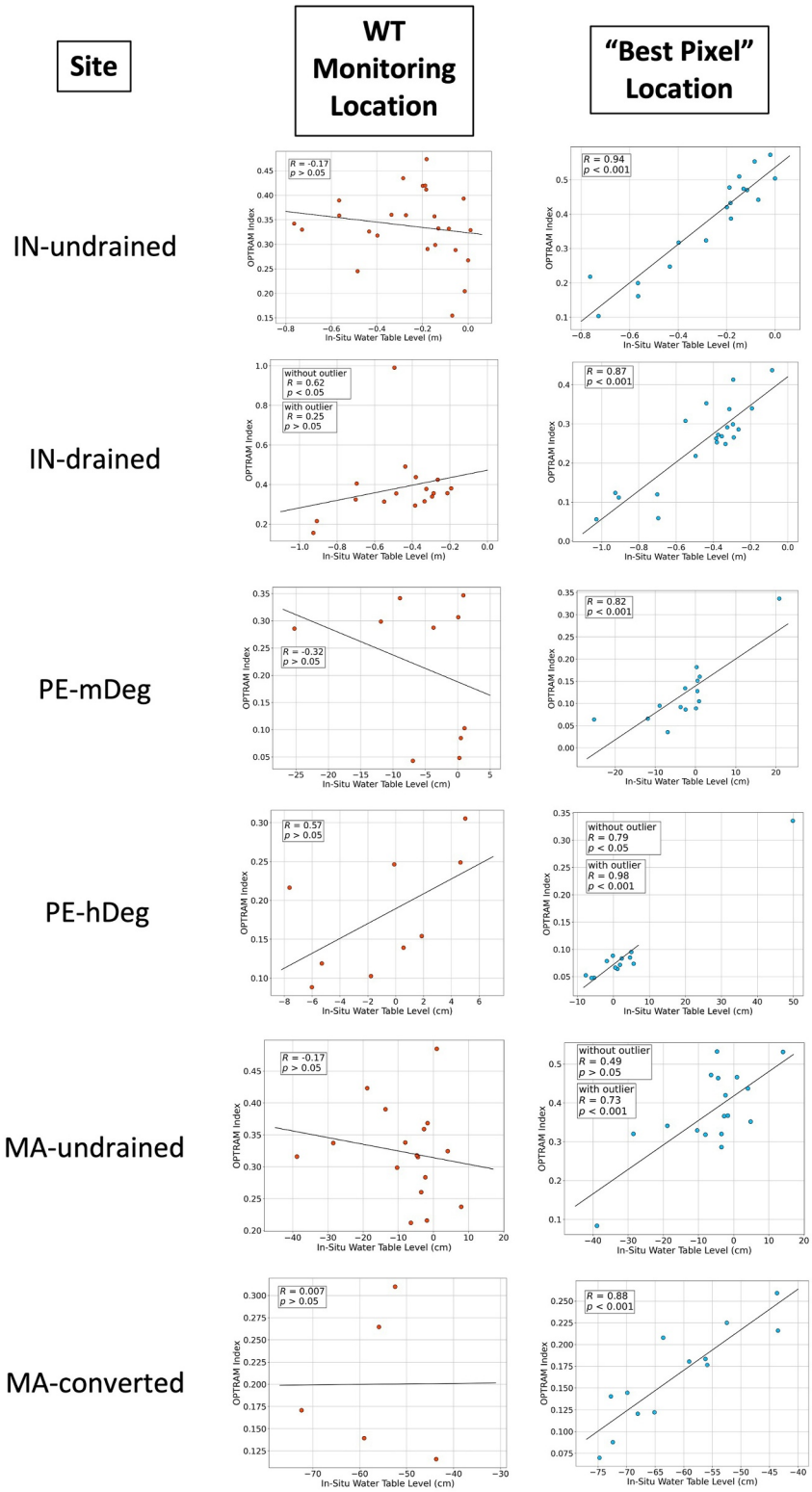

Figure 8. Scatterplots showcasing the correlation between OPTRAM index and in situ WT at each site. The red points are taken at the WT monitoring location and the blue are located at the "best pixel" location.

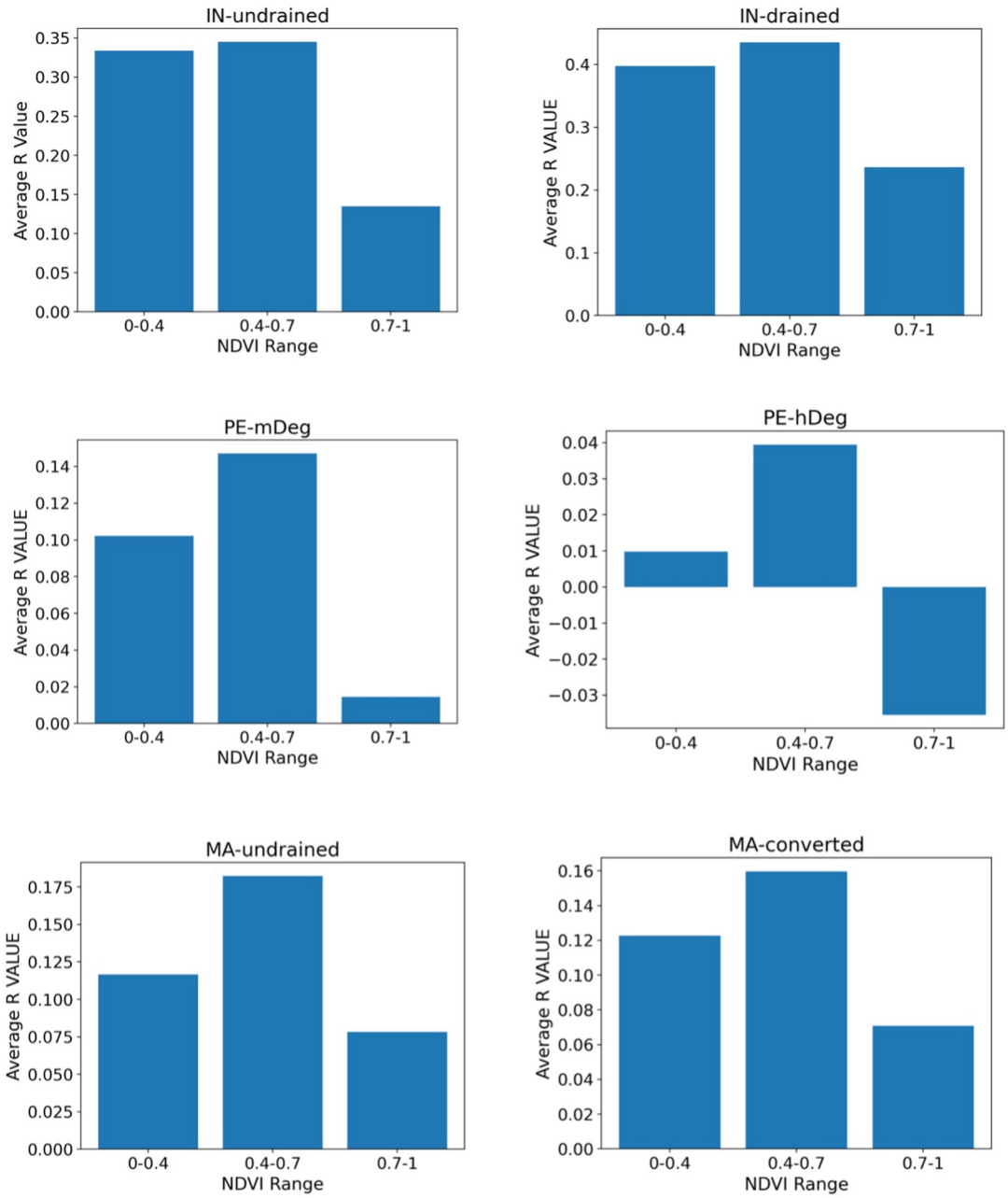

Figure 9. Histograms showing the average R-value for various NDVI classes (0–0.4, 0.4–0.7, 0.7–1) for each site. For these intervals, the lower bound is included but the upper bound is not.

3.6. Impact of El Niño and Non-El Niño Years

We could not show the significant difference between El Niño and non-El Niño years at all sites due to limited data. Here, we used the IN-undrained and IN-drained sites for this analysis. It is important to note that these sites had only 5 and 6 data points covering El Niño years, respectively. Despite Figure 10 showing different linear regression slopes for El Niño and non-El Niño years, 95% confidence intervals of these linear regression slopes are highly overlapped (Table S1).

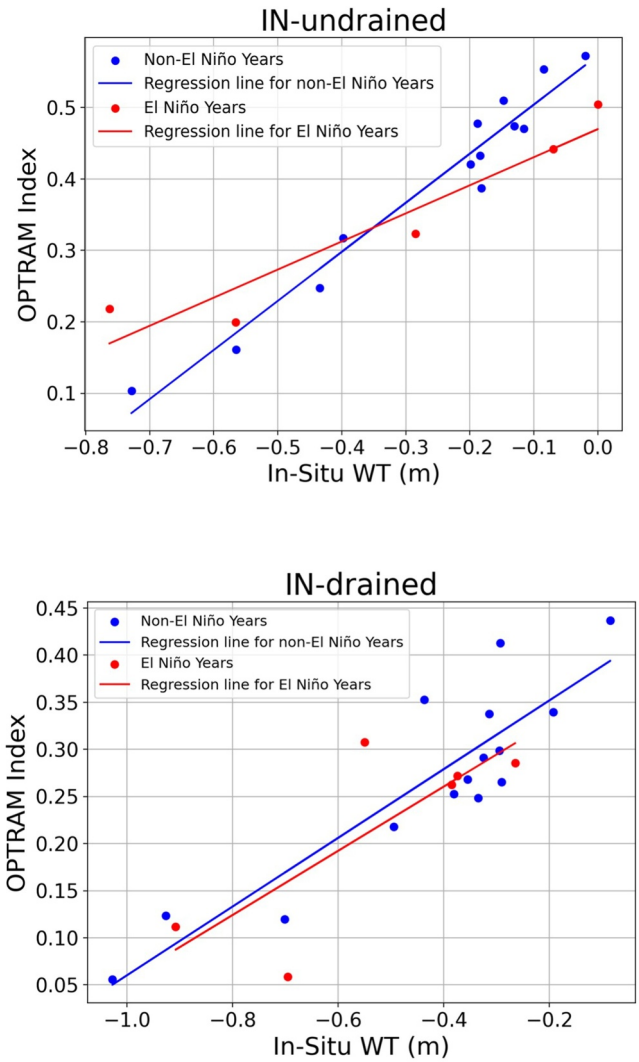

Figure 10. Scatterplot of OPTRAM versus in situ WT for IN-undrained and IN-drained. The data points and regression line are red for El Niño years and blue for non-El Niño years. These plots only show the pixel with the highest Pearson-R value.

3.7. Uncertainty in OPTRAM Index-WT Relationship

Using the cross-validation approach for each site's best pixel, we found the mean of the difference between the observed and predicted OPTRAM index values (observed OPTRAM index value minus predicted OPTRAM index value) to be 0.001, 0.0007, 0.009, 0.009, −0.003, −0.0008 for IN-undrained, IN-drained, PE-mDeg, PE-hDeg, MA-undrained, and MA-converted, respectively. The MAE was 0.044 for IN-undrained, 0.045 for IN-drained, 0.045 for PE-mDeg, 0.021 for PE-hDeg, 0.072 for MA-undrained, and 0.026 for MA-converted. The OPTRAM index is a unitless quantity and therefore MAE is also a unitless quantity. The values for the mean of the difference between observed and predicted OPTRAM index values and MAE are small relative to typical OPTRAM index values calculated in this study (∼1–3 orders of magnitude smaller).

4. Discussion

This study shows OPTRAM to be capable of reproducing tropical peatland WT in areas with low vegetation density. In particular, it will allow stakeholders to estimate changes in WT using the OPTRAM index, where an increase of ~0.1 for the OPTRAM index is approximately equivalent to a 20 cm increase in WT over minimally vegetated areas. Stakeholders may then use this information to estimate WT-dependent variables such as the magnitude of carbon emissions and the probability of fire occurrence.

Temporal variability of in situ WT was similar among sites in close proximity such as IN-undrained and IN-drained (typically following rainfall patterns), and PE-mDeg and PE-hDeg. This supported our assumption that temporal fluctuations in WT within the same tropical peatland landscape are uniform (Burdun, Bechtold, Sagris, Lohila, et al., 2020), although specific magnitudes may differ. Our results indicate that OPTRAM may potentially be used for WT estimation on different timescales, especially in areas where long-term in situ measurements are not available.

However, it is important to note that this study was carried out on a limited number of sites. Additionally, there were a limited number of observations which did not allow us to conclusively trace the effect of El Niño on OPTRAM performance.

4.1. Comparison With Past Studies

A direct comparison with past studies using OPTRAM is problematic since, to date, this is the first time this method has been used to replicate WT variability in tropical peatlands. The idea of utilizing OPTRAM for peatland WT retrieval is also in its infancy since its original intended use was for estimating soil moisture.

Our study shows that OPTRAM effectively monitors WT over areas with little to no vegetation cover. This is likely due to the vegetation moisture status of trees being less sensitive to WT fluctuations relative to that of grasses and shrubs (Burdun et al., 2023). Therefore, we posit that the model is successful even over non-tree species (i.e., shrubs, ferns, sedges, and pitcher plants).

One of the first applications of OPTRAM was in northern peatlands by Burdun, Bechtold, Sagris, Lohila, et al. (2020). This work also used the "best pixel" approach and found similar results to those found in this study—large correlations in areas with minimal vegetation cover and low correlations in areas with high vegetation cover. It was also concluded that the degree of spatial resolution affects OPTRAM performance, with higher resolutions (30-m) yielding higher R-values relative to lower resolutions (500-m). A similar study compared two trapezoid models for WT retrieval at several northern bogs (Burdun, Bechtold, Sagris, Komisarenko, et al., 2020)—namely,

OPTRAM and the Thermal-Optical Trapezoid Model (TOTRAM). Results showed that temporal correlations with in situ WT were higher using OPTRAM versus TOTRAM indices.

That study concluded that neither model could recreate the spatial variability of WT, but instead, OPTRAM was observed to perform optimally over the treeless portions of the multiple bog landscapes (Burdun, Bechtold, Sagris, Komisarenko, et al., 2020). The same result was found when testing OPTRAM at 53 northern peatland sites (Burdun et al., 2023). Specifically, OPTRAM sensitivity to WT decreased when tree cover density was 50% or more (Burdun et al., 2023). Furthermore, the lack of spatial correlation may go beyond vegetation density and occur due to differences in the WT-soil moisture relationship in certain areas. A similar result was obtained in this study when applying OPTRAM to tropical peatlands, where spatial differences in OPTRAM performance were a function of vegetation density patterns.

Another study found a combination of optical and synthetic aperture radar (SAR) (multi-sensor approach) may better resolve in situ peatland WT measurements (Räsänen et al., 2022). However, like methods solely using optical data, the same limitations were found, such as higher average regression performance over sparsely treed and open peatlands. Interestingly, it was also discovered that a multi-sensor approach performs best in undrained rather than restored peatlands (Räsänen et al., 2022), agreeing with our results when applying an optical method at tropical peatlands.

4.2. Study Limitations and Application Approaches to Other Tropical Peatlands

Due to the nature of the study area, this work is subject to limitations. First, the quality of surface reflectance data is restricted owing to the typically cloudy conditions of tropical regions. As a result, many pixels were discarded to maintain reliable calculations for OPTRAM index and NDVI. This filtering introduced many data gaps in the OPTRAM index time series. These were then exacerbated by limited temporal in situ WT at the sites. Therefore, regression analysis could not be conducted if in situ and OPTRAM index data were not available for the same timestamp, which further limited our data pool. Fortunately, this is compensated for by the high temporal representation of data points used, with a maximum of five site years of data.

Mean absolute errors (MAE) in the OPTRAM index-WT relationship were relatively small compared to OPTRAM index values, except for PE-hDeg. This potentially highlights the high uncertainty that comes with estimating WT via OPTRAM in degraded tropical peatland systems.

The lack of spatial pattern in correlations over an undrained heavily degraded forest (PE-hDeg) and a drained plantation (MA-converted) indicates OPTRAM to not be able to capture WT in areas with high disturbance and high drainage. One explanation may be that the relatively high bulk density of the upper peat layer limits horizontal water flow which affects vegetation moisture status (Burdun et al., 2023). Additionally, it may be that exceedingly low WT results in a loss of the WT and vegetation moisture status connection and therefore decreases OPTRAM performance (although this was not the case for Peruvian sites) (Burdun et al., 2023).

Many of the "best pixel" correlations at sites had notably high Pearson-R values. We caution readers not to attribute this to OPTRAM's overall effectiveness in monitoring WT. Rather, it is important to note that the main takeaway lies in the spatial distribution of the OPTRAM index-WT correlation strengths. To apply OPTRAM successfully at other tropical peatland sites, stakeholders must find either open or low-vegetated areas. We realize that some of these systems are densely vegetated, and that in most areas, OPTRAM would perform poorly. However, since the upper peat layer has high hydraulic conductivity due to saturation/inundation, temporal WT fluctuations are synchronized over several kilometers (Hergoualc'h et al., 2020; Hirano et al., 2012). This, in turn, allows OPTRAM to reproduce WT fluctuations across the landscape using only a relatively small area within the peatland. However, WT synchronization may be lost due to drainage ditches (i.e., MA-converted), which may cause unreliable OPTRAM-based estimations of peatland WT.

Even in the case of densely vegetated tropical peatlands such as PSF, one can estimate WT variations using only non-forested areas or areas with low vegetation. Furthermore, some tropical peatlands are herbaceous swamps (Hastie et al., 2022; Urbina & Benavides, 2015; Villa et al., 2019), making these locations an ideal fit for OPTRAM application.

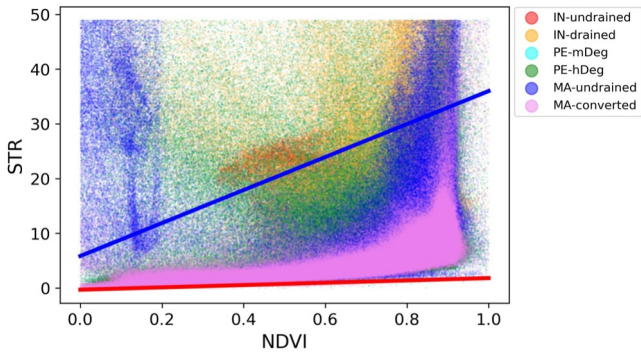

Figure 11. STR-NDVI space showing large overlap between all sites. This indicates that OPTRAM parameterization is valid for all sites. Only pixels labeled as "clear" are shown. NDVI and STR values were taken from three timesteps throughout the year (beginning, middle, and end of year) to take into account seasonality of the wet and dry seasons at each site. IN-undrained, IN-drained, PE-mDeg, PE-hDeg, MA-undrained, and MA-converted used values from 2018, 2017, 2018, 2018, 2014, and 2018, respectively. Blue line is the wet edge and red line is the dry edge.

When comparing per-pixel NDVI and R-values, we assumed tropical NDVI to experience minimal variation at each site. Therefore, we used surface reflectance values from a date in September to represent NDVI at each site. We acknowledge that tropical vegetation surface reflectance values may differ temporally due to the wet and dry seasons, so we chose the shoulder month of September to incorporate in our analyses. However, even with this approach, the reader should be cautioned when interpreting each pixel's *R* and NDVI relationship.

We can infer that pixels with high positive correlation values and high NDVI are not situated within the red clusters as shown in Figure 7. As established in the previous section, these clusters of red (high positive correlation between OPTRAM index and in situ WT) appeared in locations with low and intermediate NDVI (Figure 9). Therefore, pixels with both high Pearson-R and high NDVI are likely not included within the red pixel clusters and may instead be a speck of red within a sea of blue (negative correlation) or white (no correlation). This may be due to small data samples and spurious correlation, but future studies are encouraged to investigate further.

Future work should expand on tropical peatland WT retrieval via remote sensing through approaches that will not necessarily depend on vegetation cover and clouds. For example, the National Aeronautics and Space Administration's Soil Moisture Active Passive satellite measures soil water content in the L-band that may penetrate clouds and dense vegetation (Dadap et al., 2019), albeit with relatively coarse resolution (9 km). Leveraging these kinds of methods to also yield WT approximations must be a priority of future work, especially due to the overall limited representation in tropical peatland ecosystems.

Additionally, more on-the-ground data should be acquired in these systems to ensure the accuracy of these methods. In the context of this work, this would mean a higher temporal representation of in situ WT at tropical peatland sites to enable a more robust calculation of the OPTRAM index-WT relationship.

4.3. Implications for OPTRAM's Ability to Detect Changes in Tropical Peatland WT

Tropical peatland hydrology remains understudied relative to temperate and boreal peatlands. Our findings can open many paths to further understanding these ecosystems—from determining GHG flux magnitudes to applying OPTRAM within global models to decrease uncertainties in model output. Additionally, we obtained promising results using identical OPTRAM parameterization for all studied sites, therefore suggesting that the same OPTRAM parameterization may be applicable in other tropical peatlands. In Figure 11, the points in the STR and NDVI space overlap, meaning that OPTRAM parameterization (and therefore calibration) is valid at each site. As a result, this may be the first step toward the applicability of universal OPTRAM parameterization over tropical peatlands. OPTRAM parameterization is a time-consuming process, so a universal parameterization may greatly facilitate OPTRAM application at a global scale. This can potentially increase the spatiotemporal coverage of WT variability estimates in tropical peatlands and will only be limited spatiotemporally by the surface reflectance product in use. Additionally, we showed that the OPTRAM-WT relationship does not differ significantly between El Niño and non-El Niño years. Therefore, OPTRAM may also be used during El Niño years to provide estimates of temporal variations in tropical peatland WT. However, it is important to note that cloudy conditions characteristic of El Niño years in certain regions may result in OPTRAM being less useful. Additionally, this analysis consisted of only 5–6 data points that were within El Niño years for two study sites. Future work should therefore utilize more data in order to reach a more robust conclusion.

OPTRAM's ability to estimate changes in WT may provide stakeholders with information on past and current hotspots where peat subsidence occurs. Therefore, it may also indicate areas prone to flooding (in the event of high precipitation) and fire (in the event of low precipitation) (Ballhorn et al., 2009; Hoscilo et al., 2011; Khakim et al., 2020; Page et al., 2002; Turetsky et al., 2015). Additionally, OPTRAM may be used as a line of evidence for tropical peatland areas in need of rewetting. Owing to its vast spatial representation via remote sensing, OPTRAM

may allow stakeholders to pinpoint locations of persisting low WT. This can prompt appropriate actions to prevent the risk of high CO_2 emissions (Deshmukh et al., 2021). However, it is important to note that this would be possible if WT synchronization is not lost due to anthropogenic drainage and/or rewetting.

Based on our results, it is likely possible to capture tropical peatland WT variability for a single landscape that may span many kilometers, regardless of vegetation cover. If one section of the peatland is covered with minimal vegetation, this will suffice as an area where OPTRAM may be applied to retrieve WT variability within the entire peatland landscape. Future studies should prioritize applying OPTRAM to other types of peatlands (i.e., mountain peatlands) to determine whether a non-lowland system would yield different results. Furthermore, studies may experiment with non-linear OPTRAM parametrizations (Ambrosone et al., 2020) and new variants of OPTRAM (Sadeghi et al., 2023) to determine whether correlations with WT improve.

5. Conclusion

This study used the 30-m resolution Landsat 7 ETM+ and Landsat 8 OLI surface reflectance products to test OPTRAM's capability for monitoring WT variations in tropical peatlands. We found a positive correlation ($0.7 < R < 1$) between OPTRAM index and in situ WT in areas that had low to intermediate vegetation cover (low to intermediate NDVI). The positive correlation strength decreased and, in some instances, became negative in areas with high vegetation cover (high NDVI). At each site, the pixel associated with the location of in situ WT measurement showed relatively smaller correlation between in situ WT (apart from IN-drained and PE-hDeg where $R = 0.62$ and $R = 0.57$, respectively). Site disturbance had an effect more on the pattern of correlation distribution rather than strength, with low disturbance resulting in more structured patterns relative to sites with high disturbance. The main limitations of this study were cloud-induced data restrictions and the general lack of in situ WT data with high temporal resolution. Despite these shortcomings, our results indicate this method to be effective in monitoring tropical peatland WT variability over open and minimally vegetated areas. Furthermore, for tropical peatlands with high vegetation cover, one may apply OPTRAM to an open or minimally vegetated area to represent WT variability across the landscape.

The influence of WT on GHG emissions, surface-level peat subsidence, and fire vulnerability renders OPTRAM to be useful for understanding peatland features that are beyond hydrology. Moreover, since OPTRAM's methodology involves remotely sensed variables, one may apply this model to a broad range of tropical peatlands, including those currently not accessible by researchers. To improve on the OPTRAM method for application in tropical peatlands, future work may combine optical and SAR methods to investigate whether new approaches better reproduce in situ WT variability.

Global Research Collaboration

All principal investigators (PI) of the tropical peatland sites were included as co-authors on this study and made contributions to the manuscript. The in situ water table data in this work was used and shared online (via a public online repository) with permission from all site PIs. This includes Dr. Takashi Hirano for the Indonesian sites, Dr. Kristell Hergoualc'h for the Peruvian sites, and Dr. Guan Xhuan Wong and Dr. Lulie Melling for the Malaysian sites.

Conflict of Interest

The authors declare no conflicts of interest relevant to this study.

Data Availability Statement

Landsat surface reflectance data were downloaded from the USGS earth explorer. In situ water table data was used with permission from Takashi Hirano, Lulie Melling, Guan Xhuan Wong, and Kristell Hergoualc'h. Data for the Peruvian sites are available in Hergoualc'h et al. (2020) at https://doi.org/10.17528/CIFOR/DATA.00243. Site-scale water table data for PE-mDeg and PE-hDeg used for analysis is available in Hergoualc'h, 2024 at https://doi.org/10.6084/m9.figshare.25334854.v1. Data for the Indonesian sites are available in Hirano, 2023 at https://doi.org/10.6084/m9.figshare.22321129.v1. Data for the Malaysian sites are available in

Melling & Wong, 2024 at https://doi.org/10.6084/m9.figshare.25299358.v1. The code used for computing OPTRAM indices for each site may be accessed via https://github.com/koupsci/OPTRAM_code_updated.git.

Acknowledgments
We thank USGS for providing surface reflectance data and all members who took part in maintaining instruments at the tropical peatland sites. We acknowledge Iuliia Burdun for pioneering the implementation of OPTRAM for peatland water table retrieval. We also acknowledge support from the University of Wisconsin-Madison (UW) Center for Climatic Research, Climate, People, and Environment Program, the UW Atmospheric and Oceanic Sciences Department, the Fulbright Program, and The Malaysian-American Commission on Educational Exchange. Other financial supports include the Sustainable Wetlands Adaptation and Mitigation Program (SWAMP, Grant MTO-069018) by the United States of America and the Global Comparative Study on REDD + (Grant agreement #QZA-12/0882) by the Government of Norway, and JSPS KAKENHI Grant (JP19H05666). IB acknowledged support from the Academy of Finland funding (PEATSPEC, decision no 341963). We would also like to thank the Sarawak Tropical Peat Research Institute and the team members, Edward Baran Aeries and Joseph Wenceslaus Waili, for maintaining all the water table loggers. Pictures in Figure 4 were provided by Kristell Hergoualc'h, Lulie Melling, Takashi Hirano, and Kazuya Nishina. N.K.-A. conceptualized and wrote the manuscript. A.R.D. supervised the research and all authors provided suggestions and feedback on the manuscript. In situ water table data was provided by Takashi Hirano, Lulie Melling, Guan Xhuan Wong, and Kristell Hergoualc'h.

References

Adeolu, A. R., Mohammad, T. A., Daud, N. N. N., Mustapha, S., Sayok, A. K., Rory, P., & Stephanie, E. (2015). Investigating the influence of rainfall on soil carbon quantity in a tropical peatland. *Procedia Environmental Sciences*, *30*, 44–49. https://doi.org/10.1016/j.proenv.2015.10.008

Ambrosone, M., Matese, A., Di Gennaro, S. F., Gioli, B., Tudoroiu, M., Genesio, L., et al. (2020). Retrieving soil moisture in rainfed and irrigated fields using sentinel-2 observations and a modified OPTRAM approach. *International Journal of Applied Earth Observation and Geoinformation*, *89*, 102113. https://doi.org/10.1016/j.jag.2020.102113

Apers, S., De Lannoy, G. J. M., Baird, A. J., Cobb, A. R., Dargie, G. C., del Aguila Pasquel, J., et al. (2022). Tropical peatland hydrology simulated with a global land surface model. *Journal of Advances in Modeling Earth Systems*, *14*(3), e2021MS002784. https://doi.org/10.1029/2021MS002784

Ballhorn, U., Siegert, F., Mason, M., & Limin, S. (2009). Derivation of burn scar depths and estimation of carbon emissions with LIDAR in Indonesian peatlands. *Proceedings of the National Academy of Sciences*, *106*(50), 21213–21218. https://doi.org/10.1073/pnas.0906457106

Bechtold, M., Schlaffer, S., Tiemeyer, B., & De Lannoy, G. (2018). Inferring water table depth dynamics from ENVISAT-ASAR C-band backscatter over a range of peatlands from deeply-drained to natural conditions. *Remote Sensing*, *10*(4), 536. https://doi.org/10.3390/rs10040536

Burdun, I., Bechtold, M., Aurela, M., De Lannoy, G., Desai, A. R., Humphreys, E., et al. (2023). Hidden becomes clear: Optical remote sensing of vegetation reveals water table dynamics in northern peatlands. *Remote Sensing of Environment*, *296*, 113736. https://doi.org/10.1016/j.rse.2023.113736

Burdun, I., Bechtold, M., Sagris, V., Komisarenko, V., De Lannoy, G., & Mander, Ü. (2020). A comparison of three trapezoid models using optical and thermal satellite imagery for water table depth monitoring in Estonian bogs. *Remote Sensing*, *12*(12), 1980. https://doi.org/10.3390/rs12121980

Burdun, I., Bechtold, M., Sagris, V., Lohila, A., Humphreys, E., Desai, A. R., et al. (2020). Satellite determination of peatland water table temporal dynamics by localizing representative pixels of A SWIR-based moisture index. *Remote Sensing*, *12*(18), 2936. https://doi.org/10.3390/rs12182936

Busman, N. A., Melling, L., Goh, K. J., Imran, Y., Sangok, F. E., & Watanabe, A. (2023). Soil CO_2 and CH_4 fluxes from different forest types in tropical peat swamp forest. *Science of the Total Environment*, *858*, 159973. https://doi.org/10.1016/j.scitotenv.2022.159973

Chen, M., Zhang, Y., Yao, Y., Lu, J., Pu, X., Hu, T., & Wang, P. (2020). Evaluation of the OPTRAM model to retrieve soil moisture in the Sanjiang Plain of Northeast China. *Earth and Space Science*, *7*(6). https://doi.org/10.1029/2020EA001108

Cheong, N., Morgan, P., Tan, L., Koh, O., Ho, Lai, et al. (2019). Acute health impacts of the southeast asian transboundary haze problem—A review. *International Journal of Environmental Research and Public Health*, *16*(18), 3286. https://doi.org/10.3390/ijerph16183286

Christian, T. J., Kleiss, B., Yokelson, R. J., Holzinger, R., Crutzen, P. J., Hao, W. M., et al. (2003). Comprehensive laboratory measurements of biomass-burning emissions: 1. Emissions from Indonesian, African, and other fuels. *Journal of Geophysical Research*, *108*(D23), 4719. https://doi.org/10.1029/2003JD003704

Cobb, A. R., & Harvey, C. F. (2019). Scalar simulation and parameterization of water table dynamics in tropical peatlands. *Water Resources Research*, *55*(11), 9351–9377. https://doi.org/10.1029/2019WR025411

Cook, M., Schott, J. R., Mandel, J., & Raqueno, N. (2014). Development of an operational calibration methodology for the Landsat thermal data archive and initial testing of the atmospheric compensation component of a Land Surface Temperature (LST) Product from the archive. *Remote Sensing*, *6*(11), 11244–11266. https://doi.org/10.3390/rs61111244

Cook, M. J. (2014). Atmospheric compensation for a Landsat land surface temperature product [Thesis]. Rochester Institute of Technology. Retrieved from http://scholarworks.rit.edu/theses/8513

Dadap, N. C., Cobb, A. R., Hoyt, A. M., Harvey, C. F., & Konings, A. G. (2019). Satellite soil moisture observations predict burned area in Southeast Asian peatlands. *Environmental Research Letters*, *14*(9), 094014. https://doi.org/10.1088/1748-9326/ab3891

Dargie, G. C., Lewis, S. L., Lawson, I. T., Mitchard, E. T. A., Page, S. E., Bocko, Y. E., & Ifo, S. A. (2017). Age, extent and carbon storage of the central Congo Basin peatland complex. *Nature*, *542*(7639), 86–90. https://doi.org/10.1038/nature21048

Davies, S. J. (1999). Smoke-haze from the 1997 Indonesian forest ®res: Effects on pollution levels, local climate, atmospheric CO2 concentrations, and tree photosynthesis. *Forest Ecology and Management*, *8*.

Deshmukh, C. S., Julius, D., Desai, A. R., Asyhari, A., Page, S. E., Nardi, N., et al. (2021). Conservation slows down emission increase from a tropical peatland in Indonesia. *Nature Geoscience*, *14*(7), 484–490. https://doi.org/10.1038/s41561-021-00785-2

Dohong, A., Aziz, A. A., & Dargusch, P. (2017). A review of the drivers of tropical peatland degradation in South-East Asia. *Land Use Policy*, *69*, 349–360. https://doi.org/10.1016/j.landusepol.2017.09.035

Evers, S., Yule, C. M., Padfield, R., O'Reilly, P., & Varkkey, H. (2017). Keep wetlands wet: The myth of sustainable development of tropical peatlands - Implications for policies and management. *Global Change Biology*, *23*(2), 534–549. https://doi.org/10.1111/gcb.13422

Foga, S., Scaramuzza, P. L., Guo, S., Zhu, Z., Dilley, R. D., Beckmann, T., et al. (2017). Cloud detection algorithm comparison and validation for operational Landsat data products. *Remote Sensing of Environment*, *194*, 379–390. https://doi.org/10.1016/j.rse.2017.03.026

Gaveau, D. L. A., Salim, M. A., Hergoualc'h, K., Locatelli, B., Sloan, S., Wooster, M., et al. (2014). Major atmospheric emissions from peat fires in Southeast Asia during non-drought years: Evidence from the 2013 Sumatran fires. *Scientific Reports*, *4*(1), 6112. https://doi.org/10.1038/srep06112

Harris, A., & Bryant, R. G. (2009). A multi-scale remote sensing approach for monitoring northern peatland hydrology: Present possibilities and future challenges. *Journal of Environmental Management*, *90*(7), 2178–2188. https://doi.org/10.1016/j.jenvman.2007.06.025

Hastie, A., Honorio Coronado, E. N., Reyna, J., Mitchard, E. T. A., Åkesson, C. M., Baker, T. R., et al. (2022). Risks to carbon storage from land-use change revealed by peat thickness maps of Peru. *Nature Geoscience*, *15*(5), 369–374. https://doi.org/10.1038/s41561-022-00923-4

Hergoualc'h, K. (2020). Replication Data for: Hergoualc'h et al. (2020) Spatial and temporal variability of soil N_2O and CH_4 fluxes along a degradation gradient in a palm swamp peat forest in the Peruvian Amazon [Dataset]. *Center for International Forestry Research (CIFOR)*. https://doi.org/10.17528/CIFOR/DATA.00243

Hergoualc'h, K. (2024). Site-scale water table level at a moderately degraded and heavily degraded site within a peat swamp forest in the Northern Peruvian Amazon [Dataset]. *Figshare*. https://doi.org/10.6084/m9.figshare.25334854.v1

Hergoualc'h, K., Dezzeo, N., Verchot, L. V., Martius, C., Lent, J., Aguila-Pasquel, J., & López Gonzales, M. (2020). Spatial and temporal variability of soil N_2O and CH_4 fluxes along a degradation gradient in a palm swamp peat forest in the Peruvian Amazon. *Global Change Biology*, *26*(12), 7198–7216. https://doi.org/10.1111/gcb.15354

Hergoualc'h, K., Van Lent, J., Dezzeo, N., Verchot, L. V., Van Groenigen, J. W., López Gonzales, M., & Grandez-Rios, J. (2023). Major carbon losses from degradation of Mauritia flexuosa peat swamp forests in western Amazonia. *Biogeochemistry*, *167*(4), 327–345. https://doi.org/10.1007/s10533-023-01057-4

Hergoualc'h, K. A., & Verchot, L. V. (2012). Changes in soil CH_4 fluxes from the conversion of tropical peat swamp forests: A meta-analysis. *Journal of Integrative Environmental Sciences*, *9*(1), 31–39. https://doi.org/10.1080/1943815X.2012.747252

Hikouei, I. S., Eshleman, K. N., Saharjo, B. H., Graham, L. L. B., Applegate, G., & Cochrane, M. A. (2023). Using machine learning algorithms to predict groundwater levels in Indonesian tropical peatlands. *Science of the Total Environment*, *857*, 159701. https://doi.org/10.1016/j.scitotenv.2022.159701

Hirano, T. (2023). DailyGWL.xlsx [Dataset]. *Figshare*. https://doi.org/10.6084/m9.figshare.22321129.v1

Hirano, T., Kusin, K., Limin, S., & Osaki, M. (2015). Evapotranspiration of tropical peat swamp forests. *Global Change Biology*, *21*(5), 1914–1927. https://doi.org/10.1111/gcb.12653

Hirano, T., Kusin, K., Limin, S., & Osaki, M. (2014). Carbon dioxide emissions through oxidative peat decomposition on a burnt tropical peatland. *Global Change Biology*, *20*(2), 555–565. https://doi.org/10.1111/gcb.12296

Hirano, T., Segah, H., Harada, T., Limin, S., June, T., Hirata, R., & Osaki, M. (2007). Carbon dioxide balance of a tropical peat swamp forest in Kalimantan, Indonesia. *Global Change Biology*, *13*(2), 412–425. https://doi.org/10.1111/j.1365-2486.2006.01301.x

Hirano, T., Segah, H., Kusin, K., Limin, S., Takahashi, H., & Osaki, M. (2012). Effects of disturbances on the carbon balance of tropical peat swamp forests. *Global Change Biology*, *18*(11), 3410–3422. https://doi.org/10.1111/j.1365-2486.2012.02793.x

Holden, J., Chapman, P. J., & Labadz, J. C. (2004). Artificial drainage of peatlands: Hydrological and hydrochemical process and wetland restoration. *Progress in Physical Geography: Earth and Environment*, *28*(1), 95–123. https://doi.org/10.1191/0309133304pp403ra

Hooijer, A., Page, S., Jauhiainen, J., Lee, W. A., Lu, X. X., Idris, A., & Anshari, G. (2012). Subsidence and carbon loss in drained tropical peatlands. *Biogeosciences*, *9*(3), 1053–1071. https://doi.org/10.5194/bg-9-1053-2012

Hoscilo, A., Page, S. E., Tansey, K. J., & Rieley, J. O. (2011). Effect of repeated fires on land-cover change on peatland in southern Central Kalimantan, Indonesia, from 1973 to 2005. *International Journal of Wildland Fire*, *20*(4), 578. https://doi.org/10.1071/WF10029

Hoyos-Santillan, J., Lomax, B. H., Large, D., Turner, B. L., Lopez, O. R., Boom, A., et al. (2019). Evaluation of vegetation communities, water table, and peat composition as drivers of greenhouse gas emissions in lowland tropical peatlands. *Science of the Total Environment*, *688*, 1193–1204. https://doi.org/10.1016/j.scitotenv.2019.06.366

Huat, B. B. K., Kazemian, S., Prasad, A., & Barghchi, M. (2011). State of an art review of peat: General perspective. *International Journal of the Physical Sciences*, *9*.

Jauhiainen, J., Limin, S., Silvennoinen, H., & Vasander, H. (2008). Carbon dioxide and methane fluxes in drained tropical peat before and after hydrological restoration. *Ecology*, *89*(12), 3503–3514. https://doi.org/10.1890/07-2038.1

Joosten, H. (2009). The global peatland CO_2 picture: Peatland status and drainage related emissions in all countries of the world.

Kalacska, M., Arroyo-Mora, J., Soffer, R., Roulet, N., Moore, T., Humphreys, E., et al. (2018). Estimating peatland water table depth and net ecosystem exchange: A comparison between satellite and airborne imagery. *Remote Sensing*, *10*(5), 687. https://doi.org/10.3390/rs10050687

Khakim, M. Y. N., Bama, A. A., Yustian, I., Poerwono, P., Tsuji, T., & Matsuoka, T. (2020). Peatland subsidence and vegetation cover degradation as impacts of the 2015 El Niño event revealed by Sentinel-1A SAR data. *International Journal of Applied Earth Observation and Geoinformation*, *84*, 101953. https://doi.org/10.1016/j.jag.2019.101953

Kim, J.-W., Lu, Z., Gutenberg, L., & Zhu, Z. (2017). Characterizing hydrologic changes of the Great Dismal Swamp using SAR/InSAR. *Remote Sensing of Environment*, *198*, 187–202. https://doi.org/10.1016/j.rse.2017.06.009

Kuwata, M., Kai, F. M., Yang, L., Itoh, M., Gunawan, H., & Harvey, C. F. (2017). Temperature and burning history affect emissions of greenhouse gases and aerosol particles from tropical peatland fire: Emission from Peatland Fire. *Journal of Geophysical Research: Atmospheres*, *122*(2), 1281–1292. https://doi.org/10.1002/2016JD025897

Kwon, M. J., Haraguchi, A., & Kang, H. (2013). Long-term water regime differentiates changes in decomposition and microbial properties in tropical peat soils exposed to the short-term drought. *Soil Biology and Biochemistry*, *60*, 33–44. https://doi.org/10.1016/j.soilbio.2013.01.023

Leifeld, J., & Menichetti, L. (2018). The underappreciated potential of peatlands in global climate change mitigation strategies. *Nature Communications*, *9*(1), 1071. https://doi.org/10.1038/s41467-018-03406-6

Lestari, I., Murdiyarso, D., & Taufik, M. (2022). Rewetting tropical peatlands reduced net greenhouse gas emissions in Riau Province, Indonesia. *Forests*, *13*(4), 505. https://doi.org/10.3390/f13040505

Masek, J. G., Vermote, E. F., Saleous, N. E., Wolfe, R., Hall, F. G., Huemmrich, K. F., et al. (2006). A Landsat surface reflectance dataset for North America, 1990-2000 [Dataset]. *IEEE Geoscience and Remote Sensing Letters*, *3*(1), 68–72. https://doi.org/10.1109/lgrs.2005.857030

Meingast, K. M., Falkowski, M. J., Kane, E. S., Potvin, L. R., Benscoter, B. W., Smith, A. M. S., et al. (2014). Spectral detection of near-surface moisture content and water-table position in northern peatland ecosystems. *Remote Sensing of Environment*, *152*, 536–546. https://doi.org/10.1016/j.rse.2014.07.014

Melling, L. (2016). Peatland in Malaysia. *Tropical peatland ecosystems*, 59–73. https://doi.org/10.1007/978-4-431-55681-7_4

Melling, L., & Wong, G. X. (2024). Groundwater levels in an undrained peat swamp forest and oil palm plantation on peat in Sarawak, Malaysia [Dataset]. *figshare*. https://doi.org/10.6084/m9.figshare.25299358.v1

Melton, J. R., Chan, E., Millard, K., Fortier, M., Winton, R. S., Martín-López, J. M., et al. (2022). A map of global peatland extent created using machine learning (Peat-ML). *Geoscientific Model Development*, *15*(12), 4709–4738. https://doi.org/10.5194/gmd-15-4709-2022

Mezbahuddin, M., Grant, R. F., & Hirano, T. (2014). Modelling effects of seasonal variation in water table depth on net ecosystem CO_2 exchange of a tropical peatland. *Biogeosciences*, *11*(3), 577–599. https://doi.org/10.5194/bg-11-577-2014

Mezbahuddin, M., Grant, R. F., & Hirano, T. (2015). How hydrology determines seasonal and interannual variations in water table depth, surface energy exchange, and water stress in a tropical peatland: Modeling versus measurements: Modeling tropical peatland ecohydrology. *Journal of Geophysical Research: Biogeosciences*, *120*(11), 2132–2157. https://doi.org/10.1002/2015JG003005

Nishina, K., Melling, L., Toyoda, S., Itoh, M., Terajima, K., Waili, J. W. B., et al. (2023). Dissolved N_2O concentrations in oil palm plantation drainage in a peat swamp of Malaysia. *Science of the Total Environment*, *872*, 162062. https://doi.org/10.1016/j.scitotenv.2023.162062

Ohkubo, S., Hirano, T., & Kusin, K. (2021). Influence of disturbances and environmental changes on albedo in tropical peat ecosystems. *Agricultural and Forest Meteorology*, *301–302*, 301–302. https://doi.org/10.1016/j.agrformet.2021.108348

Page, S. E., Rieley, J. O., & Banks, C. J. (2011). Global and regional importance of the tropical peatland carbon pool: Tropical peatland carbon pool. *Global Change Biology*, *17*(2), 798–818. https://doi.org/10.1111/j.1365-2486.2010.02279.x

Page, S. E., Siegert, F., Rieley, J. O., Boehm, H.-D. V., Jaya, A., & Limin, S. (2002). The amount of carbon released from peat and forest fires in Indonesia during 1997. *Nature*, *420*(6911), 61–65. https://doi.org/10.1038/nature01131

Parker, R. J., Boesch, H., Wooster, M. J., Moore, D. P., Webb, A. J., Gaveau, D., & Murdiyarso, D. (2016). Atmospheric CH_4 and CO_2 enhancements and biomass burning emission ratios derived from satellite observations of the 2015 Indonesian fire plumes. *Atmospheric Chemistry and Physics*, *16*(15), 10111–10131. https://doi.org/10.5194/acp-16-10111-2016

Pärn, J., Verhoeven, J. T. A., Butterbach-Bahl, K., Dise, N. B., Ullah, S., Aasa, A., et al. (2018). Nitrogen-rich organic soils under warm well-drained conditions are global nitrous oxide emission hotspots. *Nature Communications*, *9*(1), 1135. https://doi.org/10.1038/s41467-018-03540-1

Price, J. S. (2003). Role and character of seasonal peat soil deformation on the hydrology of undisturbed and cutover peatlands: Peat volume-change hydrology. *Water Resources Research*, *39*(9). https://doi.org/10.1029/2002WR001302

Promsiri, P., Tekasakul, S., Thongyen, T., Suwattiga, P., Morris, J., Latif, M. T., et al. (2023). Transboundary haze from peatland fires and local source-derived PM2.5 in Southern Thailand. *Atmospheric Environment*, *294*, 119512. https://doi.org/10.1016/j.atmosenv.2022.119512

Räsänen, A., Tolvanen, A., & Kareksela, S. (2022). Monitoring peatland water table depth with optical and radar satellite imagery. *International Journal of Applied Earth Observation and Geoinformation*, *112*, 102866. https://doi.org/10.1016/j.jag.2022.102866

Ribeiro, K., Pacheco, F. S., Ferreira, J. W., Sousa-Neto, E. R., Hastie, A., Krieger Filho, G. C., et al. (2021). Tropical peatlands and their contribution to the global carbon cycle and climate change. *Global Change Biology*, *27*(3), 489–505. https://doi.org/10.1111/gcb.15408

Rosenberry, D. O., Glaser, P. H., & Siegel, D. I. (2006). The hydrology of northern peatlands as affected by biogenic gas: Current developments and research needs. *Hydrological Processes*, *20*(17), 3601–3610. https://doi.org/10.1002/hyp.6377

Sadeghi, M., Babaeian, E., Tuller, M., & Jones, S. B. (2017). The optical trapezoid model: A novel approach to remote sensing of soil moisture applied to Sentinel-2 and Landsat-8 observations. *Remote Sensing of Environment*, *198*, 52–68. https://doi.org/10.1016/j.rse.2017.05.041

Sadeghi, M., Mohamadzadeh, N., Liang, L., Bandara, U., Caldas, M. M., & Tyler, H. (2023). A new variant of the optical trapezoid model (OPTRAM) for remote sensing of soil moisture and water bodies. *Science of Remote Sensing*, *8*, 100105. https://doi.org/10.1016/j.srs.2023.100105

Šimanauskienė, R., Linkevičienė, R., Bartold, M., Dąbrowska-Zielińska, K., Slavinskienė, G., Veteikis, D., & Taminskas, J. (2019). Peatland degradation: The relationship between raised bog hydrology and normalized difference vegetation index. *Ecohydrology*, *12*(8). https://doi.org/10.1002/eco.2159

Stockwell, C. E., Yokelson, R. J., Kreidenweis, S. M., Robinson, A. L., DeMott, P. J., Sullivan, R. C., et al. (2014). Trace gas emissions from combustion of peat, crop residue, domestic biofuels, grasses, and other fuels: Configuration and Fourier transform infrared (FTIR) component of the fourth Fire Lab at Missoula Experiment (FLAME-4). *Atmospheric Chemistry and Physics*, *14*(18), 9727–9754. https://doi.org/10.5194/acp-14-9727-2014

Strack, M., Kellner, E., & Waddington, J. M. (2005). Dynamics of biogenic gas bubbles in peat and their effects on peatland biogeochemistry: Biogeochemical effects of gas bubbles in peat. *Global Biogeochemical Cycles*, *19*(1). https://doi.org/10.1029/2004GB002330

Swails, E., Hergoualc'h, K., Verchot, L., Novita, N., & Lawrence, D. (2021). Spatio-temporal variability of peat CH4 and N2O fluxes and their contribution to peat GHG budgets in Indonesian forests and oil palm plantations. *Frontiers in Environmental Science*, *9*, 617828. https://doi.org/10.3389/fenvs.2021.617828

Swails, E., Yang, X., Asefi, S., Hergoualc'h, K., Verchot, L., McRoberts, R. E., & Lawrence, D. (2019). Linking soil respiration and water table depth in tropical peatlands with remotely sensed changes in water storage from the gravity recovery and climate experiment. *Mitigation and Adaptation Strategies for Global Change*, *24*(4), 575–590. https://doi.org/10.1007/s11027-018-9822-z

Tang, A. C. I., Melling, L., Stoy, P. C., Musin, K. K., Aeries, E. B., Waili, J. W., et al. (2020). A Bornean peat swamp forest is a net source of carbon dioxide to the atmosphere. *Global Change Biology*, *26*(12), 6931–6944. https://doi.org/10.1111/gcb.15332

Tang, A. C. I., Stoy, P. C., Hirata, R., Musin, K. K., Aeries, E. B., Wenceslaus, J., & Melling, L. (2018). Eddy covariance measurements of methane flux at a tropical peat forest in Sarawak, Malaysian Borneo. *Geophysical Research Letters*, *45*(9), 4390–4399. https://doi.org/10.1029/2017GL076457

Taufik, M., Haikal, M., Widyastuti, M. T., Arif, C., & Santikayasa, I. P. (2023). The impact of rewetting peatland on fire hazard in riau, Indonesia. *Sustainability*, *15*(3), 2169. https://doi.org/10.3390/su15032169

Taufik, M., Widyastuti, M. T., Sulaiman, A., Murdiyarso, D., Santikayasa, I. P., & Minasny, B. (2022). An improved drought-fire assessment for managing fire risks in tropical peatlands. *Agricultural and Forest Meteorology*, *312*, 108738. https://doi.org/10.1016/j.agrformet.2021.108738

Thompson, D. K., & Waddington, J. M. (2013). Peat properties and water retention in boreal forested peatlands subject to wildfire: Peat properties in fire-affected peatlands. *Water Resources Research*, *49*(6), 3651–3658. https://doi.org/10.1002/wrcr.20278

Turetsky, M. R., Benscoter, B., Page, S., Rein, G., van der Werf, G. R., & Watts, A. (2015). Global vulnerability of peatlands to fire and carbon loss. *Nature Geoscience*, *8*(1), 11–14. https://doi.org/10.1038/ngeo2325

Urbina, J. C., & Benavides, J. C. (2015). Simulated small scale disturbances increase decomposition rates and facilitates invasive species encroachment in a high elevation tropical Andean peatland. *Biotropica*, *47*(2), 143–151. https://doi.org/10.1111/btp.12191

Varkkey, H. (2013). Patronage politics, plantation fires and transboundary haze. *Environmental Hazards*, *12*(3–4), 200–217. https://doi.org/10.1080/17477891.2012.759524

Vermote, E., Justice, C., Claverie, M., & Franch, B. (2016). Preliminary analysis of the performance of the Landsat 8/OLI land surface reflectance product [Dataset]. *Remote Sensing of Environment*, *185*, 46–56. https://doi.org/10.1016/j.rse.2016.04.008

Villa, J. A., Mejía, G. M., Velásquez, D., Botero, A., Acosta, S. A., Marulanda, J. M., et al. (2019). Carbon sequestration and methane emissions along a microtopographic gradient in a tropical Andean peatland. *Science of the Total Environment*, *654*, 651–661. https://doi.org/10.1016/j.scitotenv.2018.11.109

Wong, G. X., Hirata, R., Hirano, T., Kiew, F., Aeries, E. B., Musin, K. K., et al. (2020). How do land use practices affect methane emissions from tropical peat ecosystems? *Agricultural and Forest Meteorology*, *282–283*, 107869. https://doi.org/10.1016/j.agrformet.2019.107869

Wösten, J. H. M., Clymans, E., Page, S. E., Rieley, J. O., & Limin, S. H. (2008). Peat–water interrelationships in a tropical peatland ecosystem in Southeast Asia. *CATENA*, *73*(2), 212–224. https://doi.org/10.1016/j.catena.2007.07.010

Wösten, J. H. M., Ismail, A. B., & van Wijk, A. L. M. (1997). Peat subsidence and its practical implications: A case study in Malaysia. *Geoderma*, *78*(1–2), 25–36. https://doi.org/10.1016/S0016-7061(97)00013-X

Wright, E. L., Black, C. R., Turner, B. L., & Sjögersten, S. (2013). Environmental controls of temporal and spatial variability in CO_2 and CH_4 fluxes in a neotropical peatland. *Global Change Biology*, *19*(12), 3775–3789. https://doi.org/10.1111/gcb.12330

Xu, J., Morris, P. J., Liu, J., & Holden, J. (2018). Peatmap: Refining estimates of global peatland distribution based on a meta-analysis. *CATENA*, *160*, 134–140. https://doi.org/10.1016/j.catena.2017.09.010

Zaitunah, A. S., Ahmad, A. G., & Safitri, R. A. (2018). Normalized difference vegetation index (NDVI) analysis for land cover types using Landsat 8 OLI in Besitang watershed, Indonesia. *IOP Conference Series: Earth and Environmental Science*, *126*, 012112. https://doi.org/10.1088/1755-1315/126/1/012112

Zeng, Y., Hao, D., Huete, A., Dechant, B., Berry, J., Chen, J. M., et al. (2022). Optical vegetation indices for monitoring terrestrial ecosystems globally. *Nature Reviews Earth & Environment*, *3*(7), 477–493. https://doi.org/10.1038/s43017-022-00298-5